7-21-2021 1:45 PM

Developing multi-species brain-strain-based scaling law using finite element analysis.

Xingyu Liu, *The University of Western Ontario*

Abstract

To better understand traumatic brain injury (TBI), various laboratory animal experiments have been developed. However, there lacks an effective scaling to connect animal TBI models with human brain injuries. With the help of the finite element (FE) model, brain mechanical responses such as strains can be predicted, and hence can serve as a parameter to facilitate animal to human scaling, as these tissue-level strains directly link to neuronal damage. In this thesis, first, a comprehensive comparison of brain strains between animal TBI models and human TBI cases was conducted. Then, a brain-strain-based scaling law between mouse and human was developed, which could serve as a guideline for closed head neurotrauma model design. Lastly, a novel and high mesh quality marmoset brain FE model was developed, which was used to enrich scaling law to non-human primates. In summary, the comparison method, scaling law, and new marmoset FE model, all together could help better represent human real-world TBI using laboratory mouse and marmoset TBI models, hence improving prevention, diagnostics, and therapeutics.

Keywords

Summary for Lay Audience

Traumatic brain injury (TBI) posed serious threats to social and economic development. Effective prevention, diagnostics and therapeutics need to be discovered. TBI is mostly caused by rapid linear and rotational acceleration, induced by direct blunt impact to the head or neck-involved inertia loading. One of the most common pathologies is axonal injury. During the event, brain tissues experience stretch, which causes axon fibers to be damaged when exceeding their elongation limit. From the perspective of biomechanics, the strain could serve as an effective evaluator of potential brain injury severity and risk. However, the challenge is that the in vivo observation of brain strain was almost impossible due to the skull and short impact duration. Though animal TBI experiments in the laboratory offered huge amounts of data of brain response, brain strains of these animal TBI models usually remain unknown and their comparison to brain strain in human TBI needs to be investigated. The main contribution of this thesis is to look into both human and animal brain strains among both real-world impacts and laboratory settings, and then developed codes and methods to compare and scale animal head kinematics, to better understand available animal TBI and design future animal TBI that is more relevant to human TBI. By doing so, better prevention, diagnostics, and therapeutics of TBI could be developed.

Co-Authorship Statement

Chapter 2 ('Understanding strain responses during laboratory animal and real-world human traumatic brain injuries') was co-authored with Dr. Haojie Mao. Chapter 3 ('Developing Brain-Strain-Based Scaling to Inform the Clinical Relevance of Mouse Models of Concussion Induced by Rotation') was co-authored by Lihong Lu, Kewei Bian, Dr. Arthur Brown and Dr. Haojie Mao. Chapter 4 ('Development of a marmoset brain finite element model') was co-authored with Dr. Haojie Mao.

All Chapters were drafted by Xingyu Liu and modified by Dr. Haojie Mao.

Acknowledgments

Table of Contents

List of Tables

List of Figures

Acronyms

CC: Corpus callosum

CCI: Controlled cortical impact

CHIMERA: Closed-head impact model of engineered rotational acceleration

CSDM: Cumulative strain damage measure

CSF: Cerebrospinal fluid

DAI: Diffuse axonal injury

DNA: Deoxyribonucleic acid

EDHDs: Emergency department visits, hospitalizations, and deaths

FE: Finite element

FPI: Fluid percussion injury

GHBMC: Global human body models consortium

GS: Gluttonous snake

MPS: Maximum principal strain

NHP: Non-human primates

PAC: Pia arachnoid complex

TBI: Traumatic brain injury

THUMS: Total human model for safety

Chapter 1

1 Introduction

1.1 Research Rationale

Traumatic brain injury (TBI) was estimated to affect approximately sixty-nine million individuals each year around the world [1]. 22.6 percent injury-triggered death was related to TBI. Among all age groups, the highest rates of TBI-related emergency department visits, hospitalizations, and deaths (EDHDs) were seen in older adults aged ≥75 years (2.23%), followed by children aged 0-4 years (1.66%) and individuals aged 15-24 years (1.01%) [2]. TBI can be caused by an external force, rapid acceleration, penetration or blast overpressures. The severity of TBI can be categorized into mild, moderate and severe based on patient's symptoms, with 75% to 85% of TBIs being estimated to be mild [3]. The common symptoms and consequences of TBI include headache, vomiting, confusion, depression, motor disturbances, memory loss, coma, permanently disabled, and increased risk of brain injury in the future [4]. In order to find the effective prevention, diagnostics, and therapeutics for TBI, researchers have made great efforts to understand the mechanisms and neuropathologies of TBI. To this, laboratory animal TBI models have been widely used. However, there remains a critical question. How these various animal TBI models are relevant to real-world human injuries, which this thesis attempted to address based on brain biomechanics.

1.2 Head Anatomy and Brain Function

1.2.1 Human Head Anatomy and Brain Region

The brain is the most complex and delicate organ in the human body, which is surrounded by the cerebrospinal fluid (CSF), meninges and skull. The skull is one of the hardest materials in our body. There are 8 cranium bones and 14 facial bones that help to form a protecting case to seal the brain and support facial structure. The skull is composed of three layers. The inner and outer layers are cortical bones that grew firmly and compactly, and a middle diploe layer is made up of spongy cancellous bone. The CSF flows in the subarachnoid space and keeps circulating [5] and float the brain [6]. The

meninges especially the pia arachnoid complex (PAC) prevent sliding between the skull and brain, while dura adheres to the skull and connects PAC.

The brain is the softest organ in the body [7]. It consists of gray and white matter, which are both viscoelastic and nonlinear. The gray matter consists of the majority of neuron somas and capillaries, which makes it look tan during in situ observation. The color of white matter is due to a large number of myelinated axons. Gray matter locates at the out surface of the brain, coating the white matter which is mostly in the deep regions of the brain. In general, the gray matter is more responsible for everyday activities such as controlling muscle movement, sensory perception, decision making, memory and emotions [8]. While the axon fiber bundles of white matter connect various gray matter areas and transmit nerve impulses and signals at a very high speed [8].

The brain, which is the focus of this thesis, has various components (Figure 1-1). The cerebral cortex locates at the outer surface of the brain hemispheres. The folding of gyri and sulci on the brain surface helps to maximize the surface area in a limited space. There are four lobes in the cortex including the frontal lobe, parietal lobe, temporal lobe, and occipital lobe with different functions [9]. In brief, the frontal lobe is responsible for language, movement control, personality, and prospective memory. The parietal lobe takes care of sensorimotor planning, learning and spatial recognition. The temporal lobe is responsible for voice recognition and memory. The occipital lobe is responsible for visual processing. Two brain hemispheres are connected by the corpus callosum (CC), which ensures communication between both left and right sides. The surgical transection and acute infarction of CC proved the vital role of CC, which is the functional integration of cognitive, learning and motor functions [10, 11]. The thalamus and hypothalamus can be found at the brain center below the CC. The thalamocortical neurons deal with almost all sensory inputs except for smell, and then transmit signals to the cortex [12]. The hypothalamus coordinates the endocrine and central nervous system (CNS), which then controls body's temperature, hunger, thirst, fatigue, sleep and attachment behaviors [13]. The cerebellum is located at the back of the brain, and is separated from brain lobes by the cerebellar tentorium. The cerebellum occupies only one-tenth of the brain volume but contains more than half of all the motor neurons which are used to control and coordinate

motion systems at different locations [14]. The brainstem consists of the midbrain, pons, and medulla oblongata, and connects the brain and spinal cord from the foramen magnum. The brainstem controls breathing, consciousness and heart rate. These complex brain functions have motivated huge laboratory TBI studies to understand brain dysfunctions or even mortality after impacts.
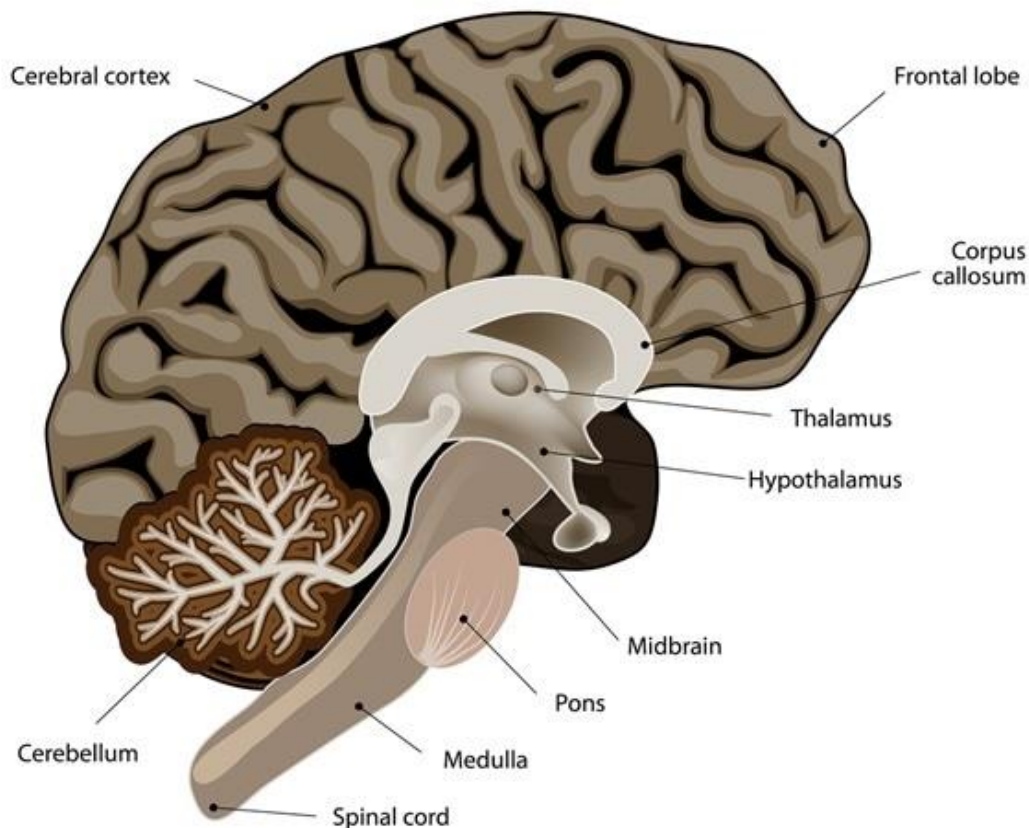
Figure 1-1 Vertical cross-section of human brain showing the cortex, corpus callosum, brain stem, cerebellum, thalamus and hypothalamus. (Image Copyright: Shutterstock)

1.2.2   Mouse Brain Anatomy

Unlike the hemispheric shape of human brain, mouse brain is slenderer along anterior-posterior direction, which makes it more sensitive to axial rotation loading than other two rotational directions. Mouse as one of the rodent species is a typical lissencephalic animal,

and the brain mass is much lower than the that of human. However, it is believed that human and mouse share 90% genes responsible for building brains and 90% genes associated with disease [15].

Mouse brains have similar anatomical components to those of humans and consists of white and gray matter, the main components are cerebral cortex, hippocampus, thalamus, cerebellum, brainstem and olfactory bulb. Like human brain, the cortex in mouse brain also controls memory [15], thalamus can be seen as the relay station for all corticopetal sensory inputs except for olfaction[16], while the cerebellum is responsible for coordination and motor actions controls [17]. The fine structure of mouse hippocampus is very similar with that of human, hippocampus supports short-term and long-term memory and spatiotemporal orientation[18]. Olfactory bulb is responsible for sense of smell, in mouse brain it accounts for 2 percent of the total volume, while the number is only 0.1 percent in human brain even the size is larger [19].
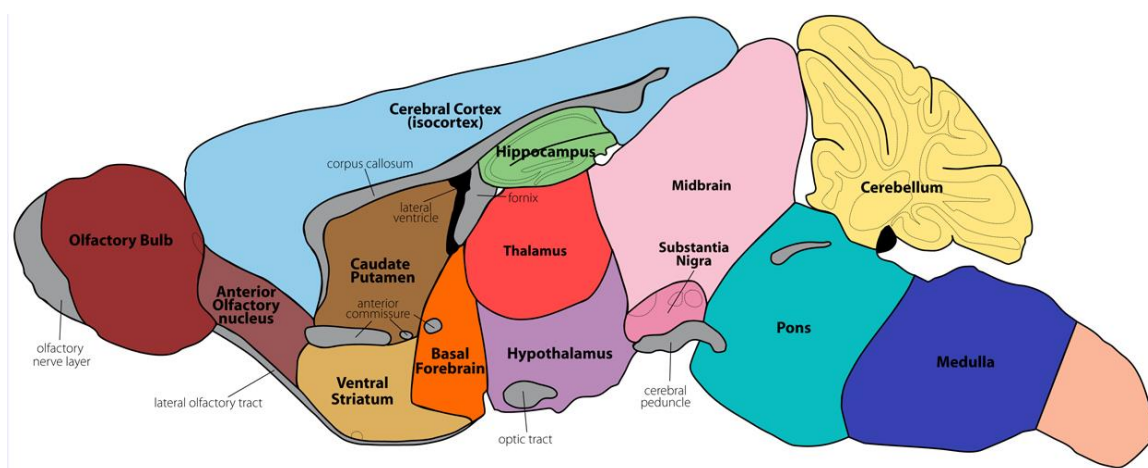
Figure 1-2 Vertical cross-section of mouse brain showing the cerebral cortex, hippocampus, thalamus, cerebellum, brainstem and olfactory bulb. (Image Copyright: The Rockefeller University)

1.3   Animal TBI Study

Animal TBI models offered huge amounts of data of the brain. Animal models can also be designed to eliminate confounding factors such as age, gender, alcohol, drug use, co-morbidities, polytrauma, and genetics, which are diverse in human samples [20].

Well-defined and clinically relevant animal models have been widely used to replicate pathological changes found in human TBI [21], find diagnostics[22], and investigate therapies [23]. Using knockout and transgenic technologies, the role of a specific gene and its corresponding function during secondary injury can be studied [24, 25]. However, there is no single animal model that is capable of describing or mimicking all pathologies of human TBI. Meanwhile, the different responses between animal and human brains cannot be neglected.

1.3.1   Rodent

Among all animal TBI models, rodents are the most popular choice since the 1990s because of their advantages such as low cost, accessibility, feasibility of the surgery, mature transgenic technology and standardized clinical outcome measurement. In general, the white/ gray matter and functional parts in the rodent brain are similar to that in the human brain. However, the rodent brain is dramatically different from the human brain in terms of geometry [26], which raises a question on how laboratory rodent TBI can mimic what a human brain has experienced during real-world traumas.

1.3.2   Marmoset

Marmoset as a non-human primate is a higher-order species than rodent, which may address the challenge of how to be more clinically relevant and successfully conduct clinical translation. From the perspective of geometry, the marmoset brain is like a smaller version of the human brain, all main anatomical components are at a similar spatial position [27]. Unlike other large animals or large primates, marmoset has a smaller size (bodyweight is around 85 to 860 grams) and quick propagation (around 144 days), which makes it suitable for animal model development. Non-human primates are needed in studying human psychiatric, neurological, and neurodegenerative disorders.

Marmoset also possesses a developed frontal lobe which is similar to human's [28]. Lastly, the genetic modification technologies were well developed for marmoset [29], which increased the potential of using marmoset as an effective brain injury model. As a result, marmoset was chosen as the animal for neuroscience research for a Japan national brain project [29].

1.4　Biomechanical Methods to Study Rodent TBI

Rodent models were able to isolate different injury mechanisms like concussion, contusion, and penetration injuries [21]. Each animal model has its inherent advantage and hypothesis. The non-uniform experiment setup could limit the significance of the comparison between experiments of the same type. The common rodent animal models for TBI include open-skull controlled cortical impact (CCI), closed-head impact model of engineered rotational acceleration (CHIMERA) and fluid percussion injury (FPI).

1.4.1　Controlled Cortical Impact (CCI)

Typical CCI is an open-skull focal injury model, first established in ferret [30], which induced focal cortical contusion. The animal subjects need to undergo anesthesia and craniotomy before the damage is induced by an electromagnetic or pneumatic impactor. The rodents were fixed in the prone position, then placed on a rigid platform with an impactor overhead. The CCI has several variables to control injury severity, including impactor tip size, impact speed, impact duration and depth.

1.4.2　Closed-Head Impact Model of Engineered Rotational Acceleration (CHIMERA)

CHIMERA [31] is one recent closed-heat impact model different from the traditional weight drop closed head model. Somehow similar to CCI, but without craniotomy, CHIMERA is a closed-head injury model with the impact being well controlled rather than dropping weights. Another advantage of the CHIMERA is that rodents were placed in the supine position with an impactor beneath, which allows the mouse head to move freely during impact.

1.4.3   Fluid Percussion Injury (FPI)

FPI induces brain tissue deformation and pressure by applying a fluid pulse to the dura of an open-skull subject. The injury severity depends on the strength of the pressure pulse [32]. In the beginning, the fluid pressure pulse was developed by transmitting the gravitational potential energy of a pendulum to a piston full of fluid. The height of the pendulum is the main controllable variable. However, the length of the saltwater cylinder and the angle between the nozzle of cylinder and skull induced complicated factors making model input hard to control. To address this, Kabadi et al.[33] created a pneumatically driven instrument that can precisely control the pressure magnitude and duration, with a goal to reduce variations among FPI experiments.

1.5   Mild TBI and Injury Evaluation Metric

One hallmark of mild TBI is diffuse axonal injury (DAI). DAI may lead to the loss of consciousness. The brain is structurally anisotropic and is full of axonal fibers. During head rotation, some regions in the brain could move faster, which could cause tension [34]. Then the axons are stretched beyond the tolerance limit. DAI injury commonly occurs during car accidents [35]. In laboratory, Bain et al [36] stretched guinea pig optical nerves and calculated a strain threshold strain of 18%.

1.5.1   Maximum Principal Strain

As previously discussed, maximum principal strain (MPS) of brain tissue was believed to be the primary brain injury mechanism [36]. The MPS was used as tissue-level predictors of brain injury in many computational studies [37, 38]. With the help of finite element analysis, the mechanical response of brain tissue during the events can be observed.

1.5.2   Strain rate

Strain rate is another injury-related load. Axon fibers are nonlinear and viscoelastic, which means axons are brittle under rapid stretch. And according to structure analysis, larger strain rate will lead to more severe axonal damage [39]. As a result, the axonal elongation rate will also determine the axon injury.

1.5.3 Cumulative Strain Damage Measure

Cumulative strain damage measure (CSDM) [40] was first introduced in the 1990's. CSDM was used in FE analysis as a biomechanical metric, which predicts brain strain-related injury risk by calculating the volume fraction of brain elements experiencing strain over the predefined threshold value.

1.6 Scaling Law

Researchers kept finding the right ways to apply animal model outcomes to human, to which scaling is essential. On the other hand, to make the findings from animal models be useful, then the designed animal head impacts should represent real-world scenarios. If the loading condition in the animal model does not take scaling into consideration, it may lead to unrealistic brain loading and inconsistent clinical outcomes compared to real-world situations [41]. The most commonly used scaling laws include mass-based scaling law [42] and equal stress/velocity scaling law [43]. It is established that brain sizes (weights) are connected with mammalian physiology [44] and tolerance of brain injury. Equal stress/velocity scaling law used kinematics as a key parameter, aiming to induce similar tissue-level mechanics for different species by changing impact strength. Recently, a novel scaling method was developed, including frequency scaling which took natural frequencies and damping ratio into scaling consideration [45].

1.7 Finite Element Model

FE model as a numerical mathematic technique has been applied to brain impact biomechanics study since the early 1970's [46]. FE models offer opportunities for researchers to look into brain responses during high-rate impacts. In addition, FEA could predict mechanics-related head injuries such as brain laceration or axon damage based on strain, pressure and stress.

In this thesis, the detailed, validated and widely used human head and mouse brain FE models were used to investigate intracranial brain mechanical response and locate the regions that are at high risk of tissue damage. This study used various human FE models, including the head FE model of global human body models consortium (GHBMC)

(Figure 1-3a), which contains key features of the brain such as the cerebral cortex, corpus callosum, cerebellum, brainstem, thalamus and ventricles. The GHBMC model was validated against intracranial pressure, brain motion, brain contusion and skull and facial response data [47]. The total human model for safety (THUMS) developed by Toyota Motor Corporation and Toyota Central R&D Labs was also used for whole-body simulation (Figure 1-3b). This model has been widely validated to produce reliable results [48]. As for the mouse brain model, it is based on the first 3D rat brain model with detailed anatomical structures and biomechanically validated [49] (Figure 1-3c). In addition, a novel marmoset brain finite element model was developed in this thesis research (Figure 1-3d), and is shown here.

All models consist primarily of hexahedral, tetrahedral and quadrilateral shell elements. The element number and element density of all the FE brain models are checked to be in the similar level. The white and gray matter and ventricle material properties of GHBMC and the mouse head model were listed in Table 1.

Table 1 Typical viscoelastic material properties for brain models

Components	Short-time shear modulus (kPa)	Long-time shear modulus (kPa)	Decay constant (ms)
GHBMC			
Cerebrum gray	6.0	1.2	80
Cerebrum white	7.5	1.5	80
CSF	0.5	0.1	80
Mouse model			
Cerebrum gray	1.72	0.51	20
Cerebrum white	1.2	0.36	20
CSF	1.0	0.3	20
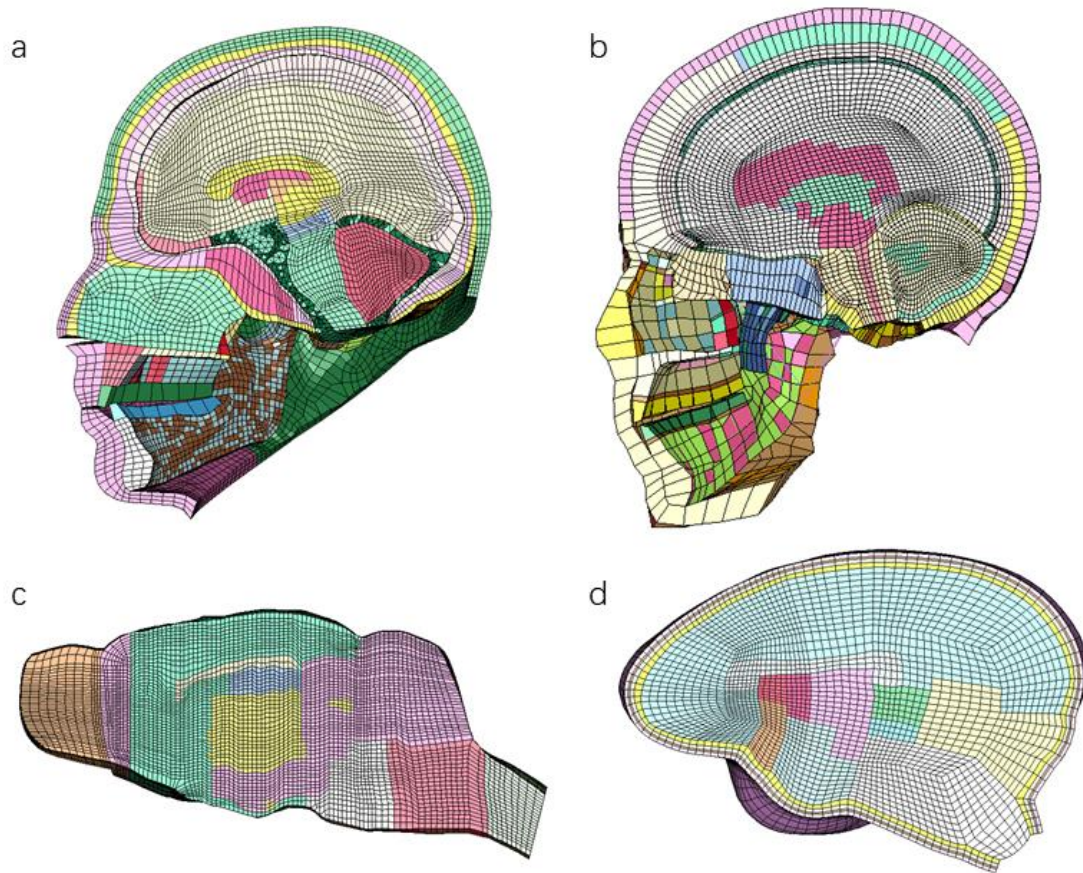
Figure 1-3 Cross-section view of different head FE models. (a) GHBMC model, (b) THUMS model, (c) Mouse model, (d) Marmoset head model developed in this thesis.

1.8   Research Scope

To better understand TBI biomechanics and improve animal model design, this thesis focused on the following main objectives.

#1 This study analyzed the brain responses of current widely used animal models from the perspective of biomechanics and evaluated how they mimic human real-world brain injury scenarios.

#2 This study developed a brain-strain-based scaling law that could serve as a guide that helps researchers to create brain injury in the mouse with brain strain loading equivalent to those experienced in real-world human head impacts.

#3 In order to study the feasibility of the non-human primate TBI model and help enrich scaling law, a marmoset brain finite element model with detailed anatomical structure was developed.

1.9 Thesis Structure

The breakdown of each chapter of this study is as follows.

Chapter one (this chapter) provides a basic overview of the problem related to laboratory animal TBI.

Chapter two evaluates commonly used rodent animal models for TBI, and compares their injury types (focal or diffuse), strain and strain rate with human real-world brain injury situations. The novel method for injury type determination is described.

Chapter three describes the development of brain-strain-based scaling law between mouse and human mild TBIs, as the stretch of axons mainly determines the injury severity. 201 simulations were conducted, and the CSDM 10 metric was used as injury evaluation. In addition, the relation between brain injury severity and rotational acceleration and duration during rotation is described.

Chapter four describes the development of a detailed marmoset brain finite element model, which is based on the brain atlas. 39 rotations were simulated to test the stability of the model and enrich scaling law into non-human primate species.

Chapter five concludes the main findings of this study, lists the limitations, introduces the future study, and summarizes the significance and novelty of this study.

Chapter 2

2 Understanding Strain Responses During Laboratory Animal and Real-World Human Traumatic Brain Injuries

2.1 Abstract

Laboratory animal traumatic brain injury (TBI) models are widely used to study real-world human TBI in lab. Traditionally, injury outcomes of animal TBI models such as neuropathology have been studied. However, whether tissue-level loading of the animal brain, which is the direct cause of neuronal damage, mimics the loading in the human brain remains to be further investigated. Hence, we compared brain strain responses among human and animal TBI cases. Four human TBI scenarios including concussive impact during football, whiplash loading, pedestrian to car impact, and drone-to-head impact were simulated. Four rodent TBI models including open-skull controlled cortical impact (CCI), closed-head impact model of engineered rotational acceleration (CHIMERA), fluid percussion injury (FPI) and in-house closed-head impact model using a CCI device were simulated. A novel data processing method named as the "Gluttonous Snake (GS)" was developed to objectively describe focal and diffuse injury types rather than a subjective evaluation. Furthermore, the strain and strain rate responses of brain tissue were compared between laboratory animal TBIs and real-world human TBIs. Results demonstrated that brain strain and strain rates for laboratory animal TBI models were in a much wider range compared to those for real-world human TBIs. Traditional open-skull CCI produced strain rates roughly 20 times higher than those experienced in the human brain. CHIMERA demonstrated strain and strain rate distributions comparable to those in human TBIs while with 6 times higher of strain rate, suggesting the advantage of using a closed-head TBI model.

2.2 Introduction

Traumatic brain injury (TBI) is induced by an external force or pressure wave to the head. For the biomechanical studies of TBI, usually, head kinematics data are measured from events such as contact sports [50, 51]. For neuropathological studies of TBI, laboratory

animal TBI models provide the major source for understanding inflammatory mediators, expression of detrimental cytokines and chemokines, axonal damage, cell death proportion, among others. In particular, the transgenic and gene targeting technologies helped study how human genes would express during secondary injury [52], which makes animal TBI models even more valuable. The most common animal TBI model is rodent TBI model due to the accessibility, low cost, and standardized outcome measurement related to rodents [53].

TBI is commonly categorized into focal and diffuse injury. This is mostly based on subjective observation. Focal brain injury is mainly caused by blunt or direct impact to the head causing damage such as contusion and subdural, epidural and intracranial hemorrhages. While diffuse brain injury can be resulted from rapid rotational motions, causing damage such as concussion and diffuse axonal injury (DAI). Focal and diffuse injuries can appear simultaneously as it was reported that 50% of the patients with moderate and severe TBI suffered a combination of focal and diffuse injury [54]. In addition, focal and diffuse injury could lead to similar clinical observations of pathologies [55]. An objective approach to quantify focal or diffuse brain responses could be helpful to provide a quantitative description of brain loading during impacts.

Brain tissue-level strain and strain rate responses directly cause neuronal damage. Axonal swellings, retraction balls, as well as an electrophysiological impairment that represents cell damage were reported when axon fibers were stretched [56-58]. The magnitudes of strain have a positive correlation with the degree of axonal injury. Besides, the magnitude of strain rate also affected brain damage [39, 56]. A larger strain rate with the same elongation led to larger von Mises strains in microtubules and a greater decrease in conduction velocity [39]. As a result, strain and strain rate are key indicators showing how well laboratory animal models mimic human real-world brain injury.

For rodent TBI models, the most popular experiment models include fluid percussion injury (FPI), open-skull controlled cortical impact (CCI) and weight-drop model [59]. During FPI, pressurized saline was injected into the brain through a craniotomy [60]. FPI induced mixed damage with cortical contusion at the contact area and diffuse injury all

over the brain [61]. During CCI, a craniotomy was performed, and an impactor hit the dura to induce contusion. A closed-head impact model of engineered rotational acceleration (CHIMERA) has been recently introduced [31], in which the animal was placed in the supine position and would rotate subjecting to a piston impact. CHIMERA produced DAI, concussion, and various functional deficits.

Human TBIs are widely seen under various scenarios. Contact sports such as football caused concussions and chronic traumatic encephalopathies (CTE) [62]. Car to pedestrian accidents also caused many brain injuries, frequently at severe levels [63]. A rear-end collision could induce whiplash injury which could affect the brain besides the neck [64]. Other less common scenarios such as drone-to-head impacts drew attention recently with an increasing number of civilian drones being used, and could also cause brain damage.

The objective of this study was to investigate and compare brain strain-related responses of laboratory animal TBI models and real-world human TBI events. The strain patterns were quantitatively analyzed regarding whether the loading is local or diffuse. The strains and strain rates between human and animal TBIs were quantified and compared.

2.3 Methods

2.3.1 Real-world Human and Laboratory Animal TBI Setting

This study simulated both human and animal TBI cases (Figure 2-1). Four human real-world brain injury scenarios were simulated, including concussion during football (Figure 2-1a), pedestrian to car impact (Figure 2-1b), whiplash during rear-end collision (Figure 2-1c), and drone to head impact (Figure 2-1d). This study also simulated four animal laboratory models including FPI (Figure 2-1e), open-skull CCI (Figure 2-1f), CHIMERA (Figure 2-1g), and a closed-head experiment using a CCI instrument (Figure 2-1h).
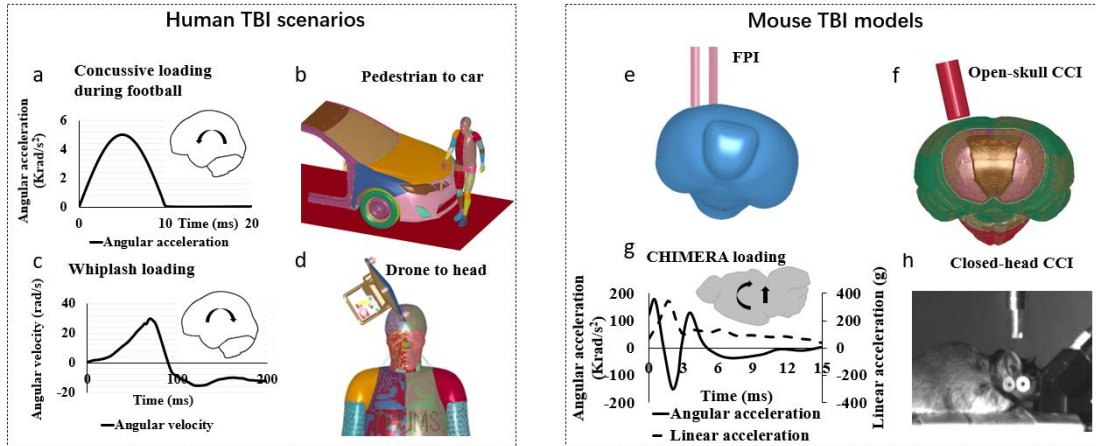
Figure 2-1 Human TBI scenarios and mouse TBI models. (a) Concussion during football, (b) Pedestrian accident, (c) Whiplash injury, (d) Drone-to-head impact, (e) CCI, (f) FPI, (g) CHIMERA, (h) In-house closed-head mouse experiment using a CCI device.

Head TBI cases referred to both literature and in-house studies. The head kinematics for the concussion was based on football [50, 65] and was simplified as a loading curve with 5000 rad/s^2 peak acceleration and 10 ms duration (Figure 2-1a). The pedestrian to car case was reconstructed from a collision between a sedan and a pedestrian with a car moving at a speed of 40 km/h (Figure 2-1b). The car FE model was based on a 2012 Toyota Camry passenger sedan (Toyota Motor Corporation, Toyota City, Japan) [66]. With 40 km/s speed, TBI is deemed as likely [67]. For whiplash loading, Siegmund et al. conducted a series of dummy rear-end collision tests [68]. According to FE analysis [69], the scene that caused the worst damage due to whiplash injury was a 15 km/h speed change in a 1998 Toyota Corolla (Toyota Motor Corporation, Toyota City, Japan) with the head restraint in the down position. The kinematics was used in this study with a rotational acceleration range between -30 to 15 rad/s (Figure 2-1c). Lastly, according to the drone impact evaluation report [70], the common quadcopter to human impact happened at lateral 58 degrees with an impact velocity of 21.9 m/s, and was simulated (Figure 2-1d).

Rodent TBI models referred to the literature. For FPI, the pressurized saline (2.6-2.9 atm) was applied to the brain surface through a nozzle with a dimeter of 3.6 mm (Figure 2-1e).

For open-skull CCI, the cylinder impactor with a diameter of 3 mm compressed brain surface at a speed of 5 m/s to the impact depth of 1 mm (Figure 2-1f). For CHIMERA [31], the peak rotational velocity was 305.8 rad/s (Figure 2-1g). For the in-house closed-head mouse experiment using a CCI device, the rotational velocity was at a mild level with a peak rotational velocity of 50 rad/s (Figure 2-1h).

Two human FE models including the Global Human Body Models Consortium (GHBMC) [71] and the Total Human Model for Safety (THUMS) [48] head models were used for human TBI simulations. The rat and mouse FE models were used for rodent TBI simulations. Strain, strain rate and cumulative strain damage measure (CSDM) were chosen to evaluate brain responses.

2.3.2   Evaluating Focal and Diffuse Brain Loading

A novel data processing method called "Gluttonous Snake (GS) was developed to distinguish focal and diffuse loading. This code rearranged the order of element strains based on strain value and element locations. There were two main laws of logic embedded in the code. First, the snakehead should always "eat" the element near it with the largest strain. Second, the snake could only go somewhere else after sweeping all elements at the focal loading spot. To achieve this, coordinates were assigned to brain elements so the code could know the spatial position of the element and calculate distance. After an initial location was picked, the code extracted all strain values near the starting point and went for the element experiencing the highest strain. At the same time, the second-highest strain values were recorded in case the snake head slipped away without recording all the high strains at one focal spot. If the recorded strains were larger than the strain near the snake head, the GS would turn back to the higher-strain element. All recorded elements will be kicked out for further loop process until all element data was rearranged. The process is visually explained (Figure 2-2).
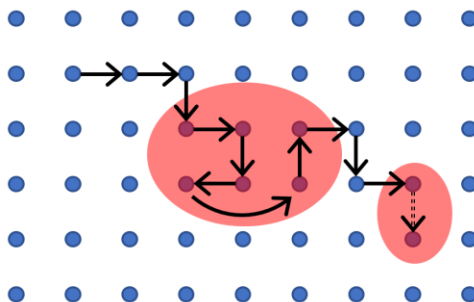
Figure 2-2 The mechanism behind the "Gluttonous Snake (GS)" method. The blue point matrix represents the sample brain elements. The red shadow areas show high strain concentration. The black arrows show the pathway (order) of how element strains are arranged, which stands for *logic law one*. The curved arrow was driven by *logic law two*. When the elements that were passed by previously experienced higher strain than the current adjacent elements, the previous scanned elements would gain new attention, making sure all elements in high strain concentration were recorded. The dotted arrow stands for a future move.

To quantify the focal and diffuse characteristics, the number of peaks above the 50th percentile strain was counted. Focal injuries should have one peak while diffuse injuries should have several peaks, with more peaks indicating more diffuse loading.

For strain and strain rate in both human and animal TBI cases, data was collected from 6 functional brain parts, including the cerebral cortex, thalamus, hippocampus, brainstem, corpus callosum and cerebellum. The strains were analyzed from Ls-PrePost output and the strain rates were calculated from the first derivative of strain time histories. All data processing was conducted in MATLAB (MathWorks, Massachusetts, USA).

2.4 Result

2.4.1 Focal vs. Diffuse

Figure 2-3 shows strain distributions using the GS method. FPI was mild with small strains less than 0.05 while these strains affected a broad range of brain tissue (Figure 2-3a), showing three peaks above the 50th percentile strain. CCI induced high strain beneath the impact center reaching over 0.3 strain, and was focal with only one peak

(Figure 2-3b). CHIMERA induced a level of strain from 0.1 to 0.2, and showed diffuse characteristics with four peaks (Figure 2-3c).
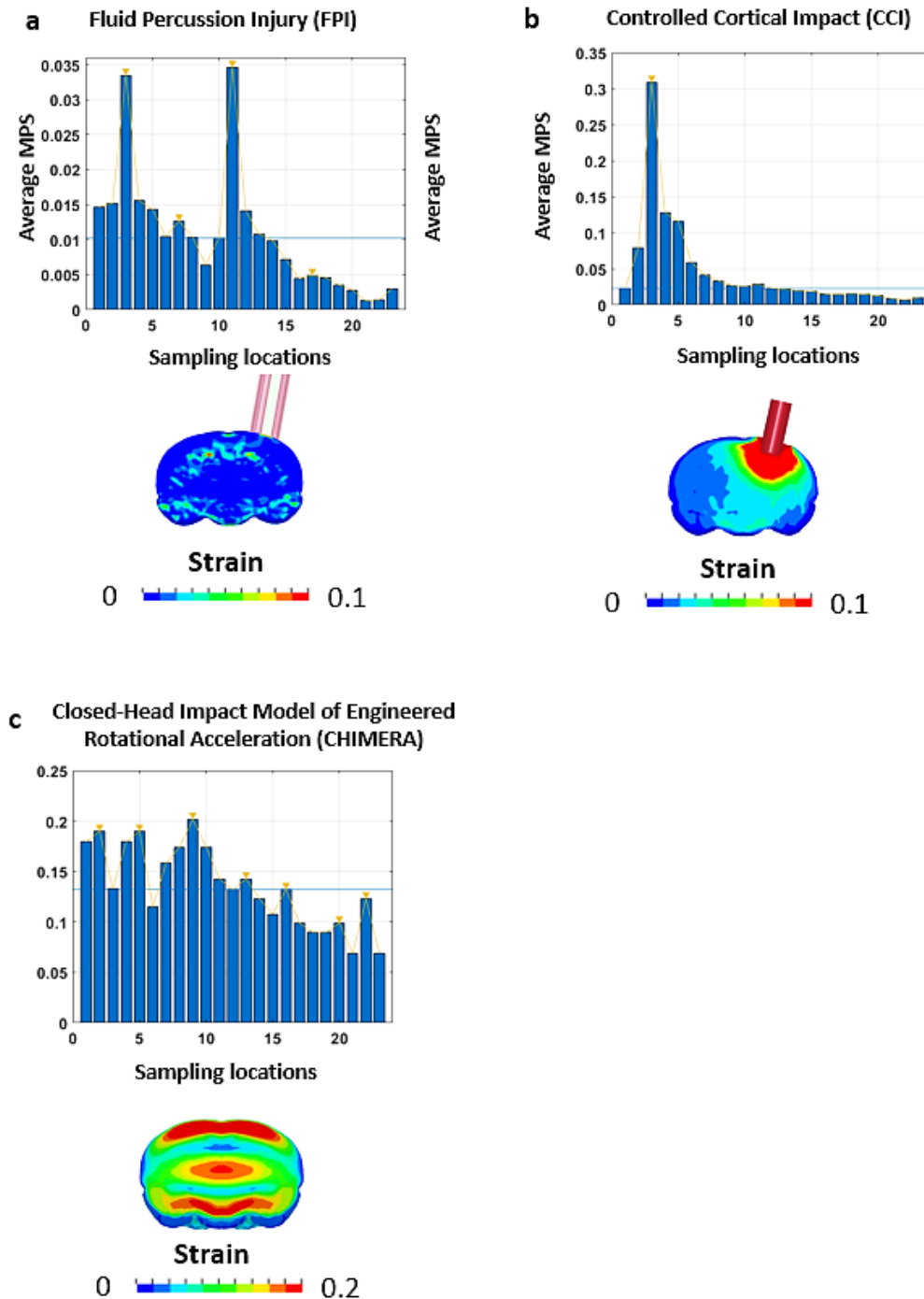
Figure 2-3 "Gluttonous Snake (GS)"-based strain distribution evaluation. (a) FPI (b) CCI and (c) CHIMERA.

Figure 2-4 shows strain distributions of human TBI scenarios. In general, all human TBI cases showed that strains were diffusely distributed. Though the level of strain in concussive loading (Figure 2-4a) was smaller than that in pedestrian to car loading (Figure 2-4b), but was comparable to whiplash loading (Figure 2-4c). Drone to head impact induced least strain (Figure 2-4d).
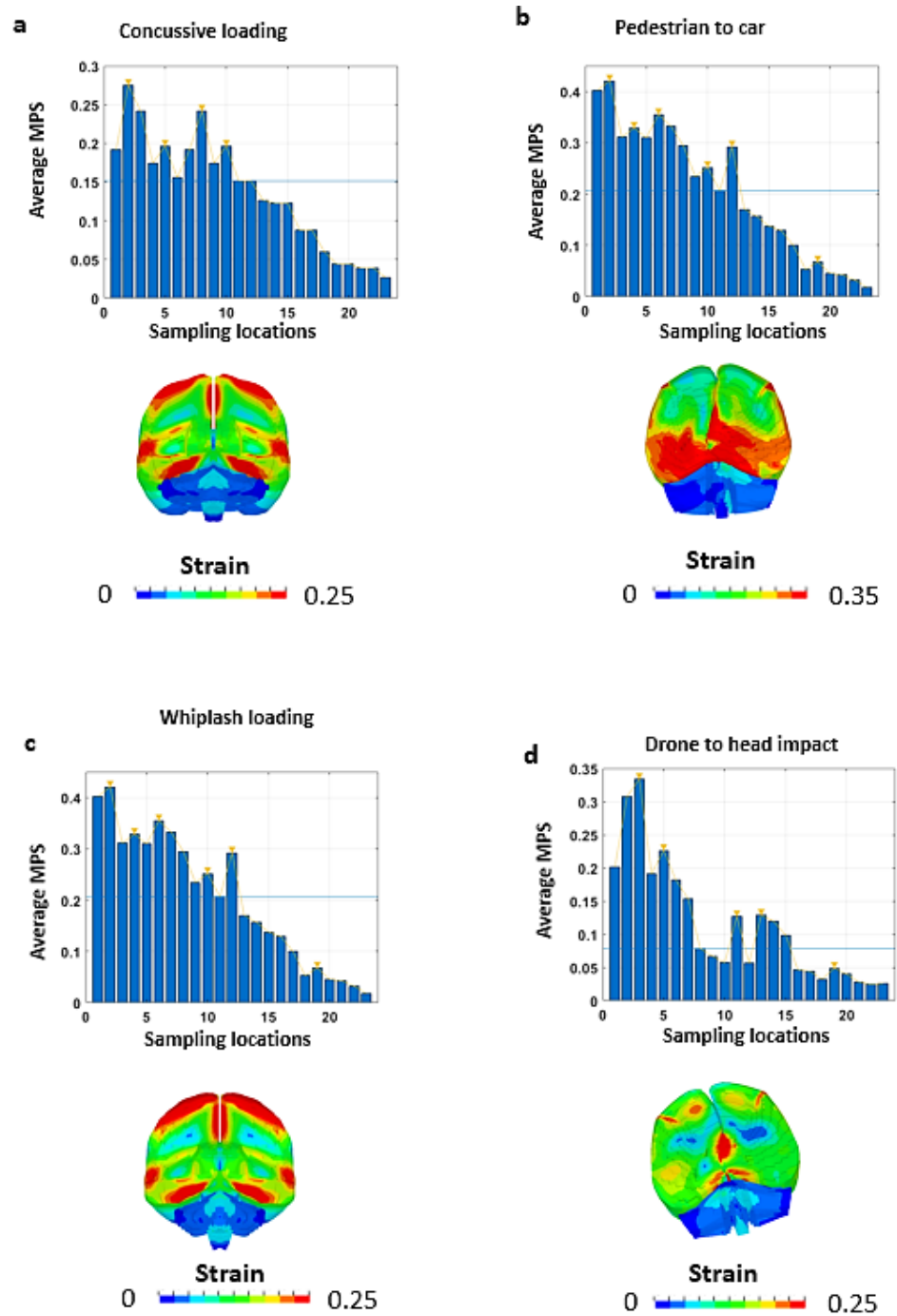
Figure 2-4 "Gluttonous Snake (GS)"-based strain distribution evaluation. (a) concussive loading, (b) pedestrian to car, (c) whiplash loading, and (d) drone to head impact.

Figure 2-5 compares the numbers of peaks based on the GS method. CHIMERA shows four peaks which were comparable to human TBI cases while CCI was focal with one peak.

The degree of brain injury diffusion
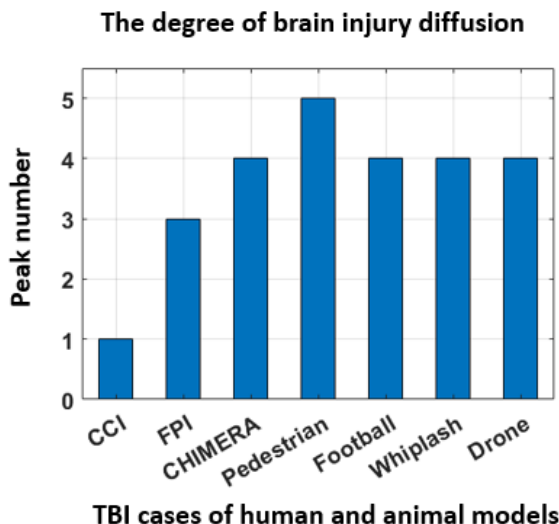
Figure 2-5 The number of peaks from the GS method.

2.4.2   Strain and Strain Rate

All human cases demonstrated relatively focused strain and strain rate ranges, while animal cases showed strains in a larger range (Figure 2-6). Concussive impact demonstrated a strain level of 0.3 while pedestrian to car impact demonstrated higher strains. Whiplash during rear-end accident had an average strain of 0.23. The average strain for the drone to human impact was 0.2. For animal TBI model, both open-skull CCI and closed-head CHIMERA provided comparable strain ranges to those in human. However, in terms of strain rate, CCI produced much higher strain rates which were almost 20 times of these experienced in human brain. Strain rates in FPI and in-house mild rotation cases were comparable to human, but at a cost of a low level of strain. At last, for CHIMERA which produced both diffuse patterns and comparable strain ranges, strain rates were still higher than those in human. Table 2 summarizes all the average and standard deviation of strain and strain rate.
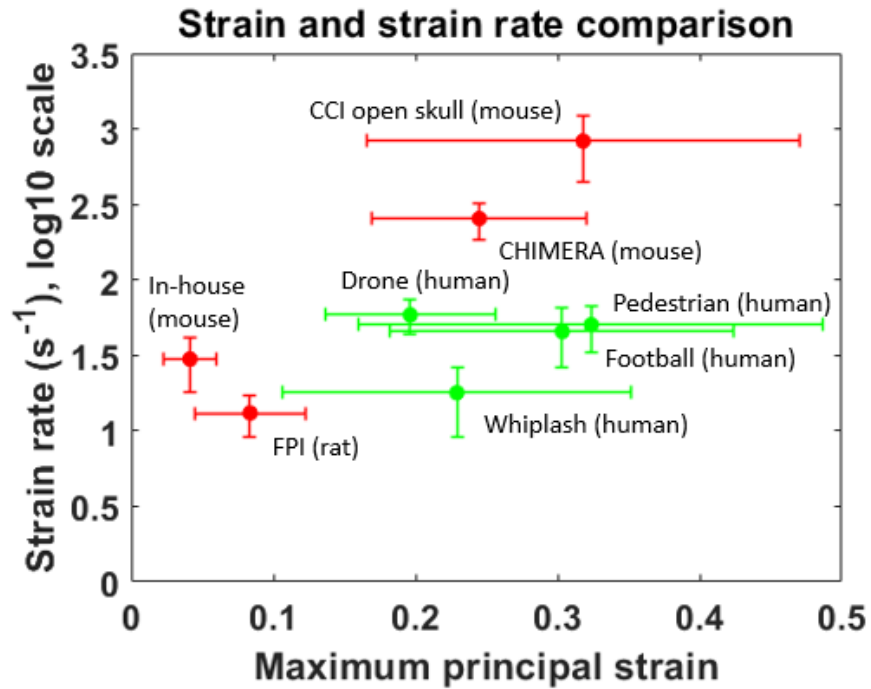
Figure 2-6 Strain and strain rate of all cases. Animal data are shown in red, while human data are shown in green. The bars stand for standard deviation.

Table 2 Average strain and strain rate with corresponding standard deviation of all cases

Case name	Strain	Standard deviation	Strain rate (s-1)	Standard deviation
Football	0.30	0.12	46	19
Pedestrian	0.32	0.16	51	17
Whiplash	0.23	0.12	18	9
Drone	0.20	0.06	59	15
FPI	0.08	0.04	13	4
CCI	0.32	0.15	832	390
CHIMERA	0.24	0.08	255	70
Small rotation	0.04	0.02	30	12

2.5   Discussion

The analysis of brain strains during four real-world human TBI scenarios and four laboratory animal TBI models was conducted. The data demonstrated that open-skull CCI

and FPI models, though commonly used, did not reproduce strain loading as those seen in real-world human. Closed-head model such as CHIMERA was found to produce a diffuse strain pattern that matched with human TBI. Moreover, the novel GS method was developed to quantitively describe the focal-diffuse loading characteristics inside the brain. Overall, the data supported the use of closed-head animal TBI models for future studies. The predicted diffuse strain pattern in human TBI and CHIMERA agreed with the findings that DAI was seen in these scenarios [54, 72].

The number of strain peaks above the 50th percentile of each case quantitively represented the degree of how diffuse the brain strain loading is. Even though the GS method was capable of distinguishing injury characteristics, the sampling resolution could be further improved in the future. For example, for the FPI analysis, the sample matrix was coarse compared to the scatted strain hot spots and hence only three peaks were picked up during the analysis.

The strain and strain rate of brain tissue during TBI events directly link to neuronal damage. Human TBI showed a strain range of around 0.2 to 0.35, while the strain rate was in the 20 to 60 per second range. For animal TBI, open-skull CCI also demonstrated comparable strain but this model mostly fits focal injury analysis with its concentrated strain loading. Moreover, the strain rates in CCI were dramatically higher (~20 times) than those in a human brain. As such, when using CCI, at least an improved version which reduced the impact speed to about one tenth of the regular speed, hence decreasing strain rate by 10 times, is recommended [73]. Overall, the closed-head animal TBI model is recommended because of the capability to produce a diffuse strain pattern that is comparable to mimic strains in human TBI.

2.6   Conclusion

By analyzing strain responses in both human and animal TBI cases, this study quantitively described the focal-diffuse characteristics and strain/strain rate responses of the brain. Besides, this study developed an objective method to analyze the focal-diffuse characteristics of brain loading. The data demonstrated that widely used open-skull CCI model could produce sufficient strain to brain tissues but also yielded 20 times high strain

rate compared to human TBI. The data also showed FPI might not be ideal at least for studying strain-related damage. Closed-head model like CHIMERA is recommended because of its capability to produce diffuse patterns and reasonable brain strains.

Chapter 3

3 Developing Brain-Strain-Based Scaling to Inform the Clinical Relevance of Mouse Models of Concussion Induced by Rotation

3.1 Abstract

Laboratory animal experiments are an invaluable tool for studying mild traumatic brain injury (mTBI)/concussion. Among them, rodent neurotrauma experiments have been most widely used, as transgenic and gene targeting technologies in mice allow us to test the roles of different genes in recovery from brain injury. Furthermore, the clinical relevance of rodent concussion studies can be improved by using these technologies to study concussions in animals that carry the human versions of genes known to play a role in neurological disease. However, delivering concussion injuries to the mice that are relevant to real-world human head impacts is challenging, as the mouse and human heads are dramatically different in shape and size. In the vast majority of mouse concussion experiments, the pathological and behavioral consequences of the injuries are evaluated without considering whether the injury model produces brain stretches (maximum principal strains) of the same magnitude as those experienced by human brains.

We conducted a total of 201 computational simulations to understand both human and mouse brain strains that are directly linked to neuronal damage during closed-head concussive impacts. To represent real-world human head impacts we simulated mouse head impacts with durations of 1.5 ms (Type 1 scaling), followed by simulations with durations between 1 and 2 ms (Type 2), and finally, simulations with durations from 0.75 to 4.5 ms (Type 3) to develop scaling between human and mouse, as well as to reveal the predicted effects of small and large changes in impact durations on brain strain. Guided by these simulations we calculated that desired peak rotational velocities in mice could be achieved by scaling human peak rotational velocities with factors of 5.8, 4.6, and 6.8, for flexion/extension, lateral bending, and axial rotation, respectively, to reach equal brain strains between human and mouse. The effects of impact durations on scaling were

also calculated and longer-duration mouse head impacts needed larger scaling factors to reach equal strain. The scaling method will help us to create brain injury in the mouse with brain strain loading equivalent to those experienced in real-world human head impacts.

3.2   Background

Traumatic brain injury (TBI) is one of the leading causes of death and disability around the world, and occurs in more than 2.87 million people in America every year [2]. Patients with TBI may suffer from physical, cognitive, social, emotional, and behavioral symptoms, and serious TBI can cause permanent disability and death [74]. While symptoms in mild TBI (mTBI) patients typically resolve within 7 to 10 days post-injury [75], 15% of mTBI patients go on to develop post-concussion syndrome and long-term cognitive impairment [76]. Animal studies of mTBI are actively being pursued to understand the pathophysiological underpinnings of concussion and post-concussion syndrome.

There are various types of animal TBI experiments reported in the literature, partially because of the variability in human TBI that is being modeled. Researchers have focused on three models including open-skull cortical impact injury (CCI), open-skull fluid percussion injury (FPI) and closed-head weight drop–impact acceleration injury [53]. Open-skull TBI using the cortical impactor has been popular as it allows direct loading to the brain tissue and induces high brain strain above 0.30 to the underlying cortical layers [77]. Open-skull TBI using the FPI also induces high strain up to ~ 0.1 and high pressure of approximately 180 kPa [61]. Despite the greater convenience of open-skull TBI, closed-head TBI is considered more clinically relevant because it does not require a craniotomy [78] and real-world mTBI/concussions happen with closed-skull conditions. Hence, closed-head models have been prioritized in mTBI/concussion investigation with a majority of studies using rodents [31, 79, 80]. The challenge is to ensure the mechanical loadings that rodent brains experienced in the laboratory setting are relevant to those experienced by human beings during real-world impacts.

It is well established that brain sizes are connected with mammalian physiology [44, 81]. Thus, one method that has been used to scale brain injuries between species has focused on the effects of mass [42]. Primates that have similar brain shape to human and Ommaya et al [42] reported that the risk of producing concussion in humans and primates is related to brain mass, which is determined by brain size. In studying blast injuries, Bowen et al [82] scaled the duration of the positive phase and the maximum reflected overpressure of air blast to get the same biological response among 13 species, by using scaling factors including body mass and ambient pressure. Wood et al [83] re-examined the allometric relationship between physiological manifestation and body mass across species, and came up with a new law that scales the duration of air blast using a ratio of reference mass to target animal mass using apnea data as injury evaluations.

There are also methods for scaling TBI between species that focus on parameters beyond brain mass. Takhounts et al [43] adopted a scaling law that scaled the amplitude and time of the loading condition to generate equal stress/velocity in two models of injury. Jean et al [84] focused on blast-induced TBI and emphasized that the human brain was more sensitive to blast than other mammalian species and proposed a scaling law taking relative acoustic impedance and surrounding protective structures into consideration. Saunders et al. developed a scaling rule based on the comparison between responses of two finite element (FE) models to fifteen available injury metrics [85]. A recent study conducted by Wu et al. compared four scaling laws, including one self-developed, frequency-based method, by comparing the calculated brain strains using human, macaque, and baboon brain FE models [45].

Given the lack of scaling laws between human and mouse for mTBI studies, our goal was to devise a scaling factor to translate the kinematics of human head impacts to the kinematics in laboratory mouse impacts producing similar or equivalent degrees of brain strain. We first evaluated traditional mass-based scaling and equal stress/velocity scaling methods and found that they were not accurate in scaling human to mouse mTBI. We then compared strain-based injury metrics, including cumulative strain damage measure (CSDM)10 and average strain, to identify pairs of different rotational loading conditions predicted to result in similar brain strains in human and mouse (difference < 3%). These

analyses have led us to propose scaling laws in three rotational axes that will provide a useful and efficient reference when evaluating the clinical relevance of mouse mTBI experiments and when comparing the results of mouse mTBI experiments across laboratories [47].

3.3   Methods

3.3.1   The Finite Element Human Brain and Mouse Brain Models and Simulations

The human FE brain model was developed from detailed computed tomography (CT) and MRI scans of an average adult male [47], using feature-based multi-block technology [86] to efficiently create high-quality hexahedral elements for the cerebrum, cerebellum, brainstem, corpus callosum, ventricles, and thalamus. The model was validated and exercised based on the experimental data of thirty-five cases and currently serves as one of the most used human head models to study brain responses [47]. The mouse FE brain model includes the olfactory bulb, cerebral gray matter, corpus callosum, brainstem (midbrain, pons, and medulla oblongata), cerebellum, lateral ventricle, 3rd ventricle, 4th ventricle, internal capsule, external capsule and part of spinal cord. Hexahedral meshes were used to ensure the accuracy of simulation. The mouse brain FE model has been used previously to successfully predict brain damage after experimental TBI [73, 87]. All the simulations were processed in HyperMesh (Altair Engineering, Troy, MI) and LS-PrePost, and computed in LS-DYNA (Livermore Software Technology Corporation, Livermore, CA). Acceleration loading curves were adjusted based on the unit used by the models and applied to the center of gravity of each model using *BOUNDARY_PRESCRIBED_MOTION keyword to induce flexion, lateral bending, and axial rotation.

Brain model materials, rational of kinematic loading condition to the model, and post-processing were consistent among the human and mouse. A linear viscoelastic (LVE) constitutive model for brain material properties was used in human and mouse finite element models. Although the human skull structures were modeled, these bony structures were treated as rigid for prescribed rotational loading, which is consistent with

the loading condition to the mouse brain model for which a rigid skull layer was used to prescribe head rotations. The maximum principal (tensile) strain (MPS) was calculated for both the human and mouse brain, as brain tensile strains were found to be related to neuronal damage [36, 88]

3.3.2   Real-World-Relevant mTBI Loading Condition

Extensive measurements of human head kinematics are available. Specifically, Rowson et al [65] created a large data set of human head six degrees of freedom acceleration of 1712 impacts by mean of installing accelerometers into the helmets of collegiate football players in 2007 and reported an average injury duration of 14 ms from 1712 cases. In 2012, Rowson et al [50] applied the same method to a study of 335 football players. In this study 300,977 sub-concussive and 57 concussive head impacts were detected and recorded. For concussive impacts, the average rotational acceleration was 5,022 rad/s^2. Based on the rotational head kinematics observed in these two experiments, and on the rotational acceleration versus time graph of National Football League (NFL) reconstructed impacts obtained using the six degrees of freedom (6 DOF) device [89] and Head Impact Telemetry (HIT) System [90], the acceleration loading condition for human mTBI is set to be half sinusoidal curve with the peak acceleration of 5,000 rad/s^2 and duration of 10 ms and 15 ms. Based on previous simulations, a theoretical sinusoidal curve could be used to produce similar brain strains compared to the complex kinematics curves [91]. Meanwhile, although head impacts induced both linear and rotational kinematics, it's found that rotational kinematics was responsible for generating over 95% of brain strain [91] and hence was the focus of this study.

3.3.3   Evaluating Traditional Mass-Based and Equal Stress/Velocity Scaling Laws

The human head kinematics was scaled to mouse head kinematics based on traditional laws, and then applied to the mouse FE brain model to quantify predicted strain responses.

3.3.3.1   Mass-Based Scaling Law [42, 92]

Brain mass-based scaling law focuses on the ratio of brain mass across species. Firstly, the mass of human brain model is 1256 grams [47], while the mouse brain model mass is

0.410 grams [87]. According to the scaling law, the duration and the peak acceleration scaling factors were calculated based on the brain mass ratio between human and mouse as equations (1) (2) and (3) shown below

$$\lambda_M = \frac{M_h}{M_m} = \frac{1256}{0.410} = 3063 \tag{1}$$

$$\lambda_a = \lambda_M^{-\frac{2}{3}} = \lambda_L^{-2} = (3063)^{-\frac{2}{3}} = 0.00474 \tag{2}$$

$$\lambda_T = \lambda_M^{\frac{1}{3}} = \lambda_L = (3063)^{\frac{1}{3}} = 14.5 \tag{3}$$

After this, the scaling factors were applied to human loading condition, the results are shown below

$$\text{Peak acceleration for mouse} = \frac{5000 \ (human)}{\lambda_a} = \frac{5000}{0.00474} = 1055 \ \text{Krad/s}^2 \tag{4}$$

$$\text{Duration for mouse} = \frac{10 \ (human)}{\lambda_T} = \frac{10}{14.5} = 0.6897 \approx 0.69 \ ms \tag{5}$$

3.3.3.2   Equal stress/velocity scaling law [43, 93]

This scaling law focuses on the ratio of brain geometry. The length ratio of the brain equals the cube root of mass ratio.

$$\lambda_L = \lambda_M^{\frac{1}{3}} = (3063)^{\frac{1}{3}} = 14.5 \tag{6}$$

$$\text{Peak rot acceleration for mouse} =$$
$$5000 \ (human) * \lambda_L * \lambda_L = 5000 * 14.5 * 14.5 = 1055 \ \text{krad/s}^2 \tag{7}$$

$$\text{Duration for mouse} = \frac{10 \ (human)}{\lambda} = \frac{10}{14.5} = 0.69 \ ms \tag{8}$$

In brief, despite different calculation procedures, the mass-based and equal-stress/equal-velocity-based models predicted the same kinematic parameters (peak acceleration and duration) would produce TBIs in the mouse equivalent to the average human TBI with a peak acceleration of ~5000Krad/s[2] as reported by Rowson [50].

3.3.3.3 Developing Scaling Law Based on Brain Strain: Calculation of CSDM and Average Values (Type 1 with Fixed Time Duration)

In mTBI, one of the most common and vital pathologic mechanisms is axonal damage [94]. Cater et al [88] calculated the cell loss of hippocampal slice cultures which experienced 30 different loading conditions expressed by the combinations of strain and strain rate and proved that the long-term responses of brain tissue to mechanical loading are correlated with strain instead of strain rate. Hence, we used the CSDM metric to calculate the loading to the whole brain. Equation (9) shows the formula for calculating the CSDM value.

$$\text{CSDM x} = \sum volume\ of\ element\ experienced\ strain\ more\ than\ x\% \qquad (9)$$

In an *in vivo* experiment, Bain et al [36] generated electrophysiological impairments by stretching guinea pig optical nerves with a final threshold strain of 18%. Three days later the guinea pigs were euthanized, and their optic nerves were evaluated for the presence of axonal bulbs. At an 18% strain threshold, morphological and functional axonal damage was observed. In this study, a CSDM of 10 was chosen when comparing mechanical response of brain tissue between mouse and human to be certain of setting a lower threshold for a strain that likely produces pathology significant enough to be clinically relevant. Besides CSDM10, the average strain which roughly represents the loading to the entire brain was also used. The CSDM-predicted values for all cases are calculated through an in-house program previously described [95].

The goal of mouse experiments was to yield kinematic curves generating the same CSDM values between the human and mouse. The entire process is described in Figure 3-1. The rotational acceleration curves from real-world situations were simplified as sine curves and these curves were prescribed to human brain model to analyze brain tissue stretches (Figure 3-1). We then used the duration of mTBI in the mouse as 1.5 milliseconds (Type 1 scaling) as has been reported in mouse mTBI kinematic studies [96, 97] and started with an initial guess of mouse head rotational accelerations at 190 $krad/s^2$. Then we predicted mouse model brain strain severity to the targeted human brain loadings, and adjusted rotational acceleration up or down based on the comparison,

and solved the updated loading condition on mouse brain (Figure 3-1). Finally, scaling laws were evaluated and developed when equivalent strains of the human and mouse brains were reached (Figure 3-1).
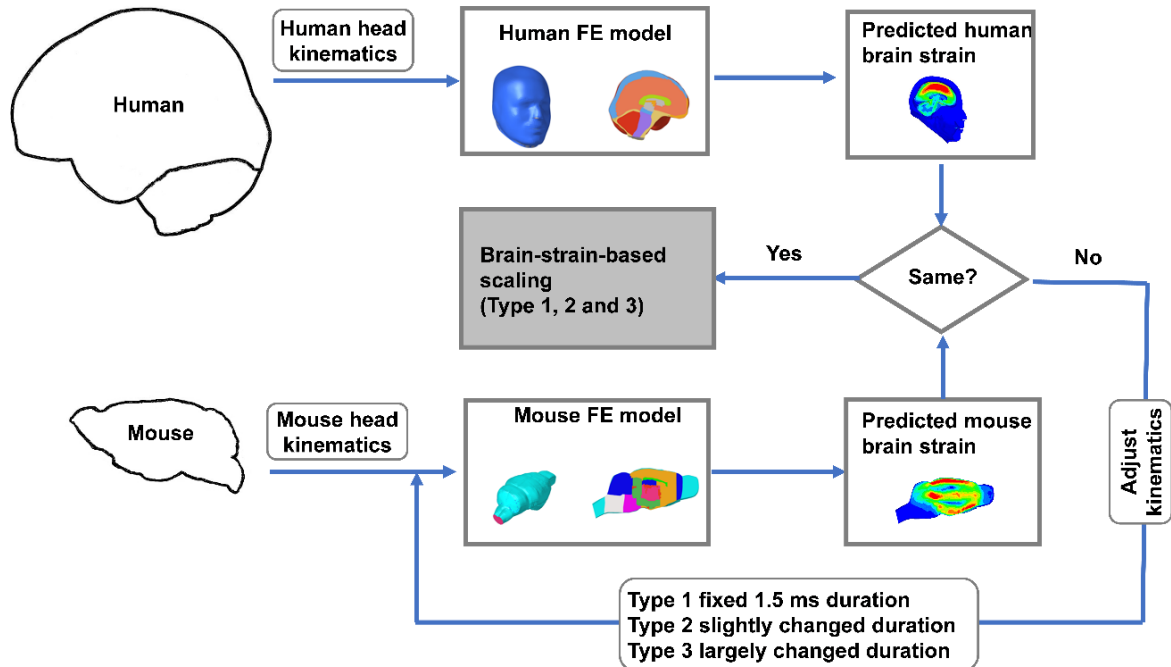
Figure 3-1 Workflow diagram represents methods in step how brain-strain-based scaling law was developed. Finite human brain and mouse brain finite element (FE) models were used to transfer head kinematics to brain strains. Three types of scaling with Type 1 indicating fixed 1.5 ms duration, Type 2 indicating slightly changed duration, and Type 3 indicating larger changed duration.

3.3.3.4 Developing Scaling Law While Considering the Effect of Varying Durations (Type 2&3)

In general, the same process (Figure 3-1) was adopted while in Type 2 scaling, time durations were slightly varied from 1 to 2 ms, and in Type 3 scaling, time durations were largely varied from 0.75 to 4.5 ms.

Slightly Changed Time Duration (Type 2): Kinematic studies of head injury have shown that peak rotational velocity has a much stronger correlation with brain strain metrics such as CSDM, than either rotational acceleration or linear kinematics [38, 91, 98-100]. Hence, rotational velocity was chosen as the primary factor for scaling. A scaling law for

rotational velocity will have a range of applications because an infinite combination of amplitudes and durations can produce the same velocity. As a result, the duration of an injury is also a significant factor when devising scaling laws. In order to make the scaling law practical and universal, to allow experimentalists to realize these kinematics parameters, a new group of simulations were conducted to explore applicable duration ranges. The acceptable tolerance was set to be less than a 3% difference between human and mouse in terms of brain strain measured using CSDM10.

Mouse model with human brain material: Since brain material properties are age-related [101] and brain material properties reported in the literature vary among researchers [102, 103], an independence test for brain materials was further conducted by applying human brain material properties to the mouse head model. This method can help understand the effect of shape and size without being affected by material diversity.

Largely Changed Time Durations (Type 3): Given the fact that there are laboratory mouse experiments performed with time durations that do not fall between 1 and 2 milliseconds [31, 104, 105], the Type 3 study was conducted with an objective to understand how large changes in injury duration might affect the brain-strain-based scaling law. To minimize computational cost only 3 impact durations of 0.75, 3, and 4.5 milliseconds were simulated.

3.4   Results

In total, 201 simulations were computed (Table 3): 3 for typical human mTBI-relevant head impacts, 2 for evaluating the current mass-based and equal stress/velocity scaling laws, 77 for developing scaling factors based on brain strain at an injury duration of 1.5 ms (Type 1), 75 for identifying the effect of small changes in injury duration (Type 2), and 22 for evaluating the effect of large changes injury duration (Type 3). A typical human or mouse head injury simulation took 2 CPUs approximately 8 hours to complete. All simulations terminated normally.

Table 3 Simulations breakdown. HMP: human material property

Study	FE Model	Rotational axis	Simulation numbers	Total simulation numbers
Human mTBI	Human model	Flexion	1	3
		Lateral bending	1	
		Axial rotation	1	
Evaluating traditional scaling laws	Mouse model [73, 87]	Flexion	1	2
Type 1 - 1.5 ms	Mouse model	Flexion	12	77
		Lateral bending	19	
		Axial rotation	22	
	Mouse model with HMP	Flexion	8	
		Lateral bending	9	
		Axial rotation	7	
Type 2 - duration slightly changed	Mouse model	Flexion	10	75
		Lateral bending	16	
		Axial rotation	10	
	Mouse model with HMP	Flexion	12	
		Lateral bending	12	
		Axial rotation	15	
Type 3 - duration largely changed	Mouse model	Flexion	11	44
		Lateral bending	22	
		Axial rotation	11	
Total				201

3.4.1 Evaluation of Traditional Scaling Laws

The typical loading condition for mTBI and the corresponding loading condition scaled from it were applied to the human and mouse brain FE models. The CSDM10 metric, which quantified the volume of brain elements experiencing principal strain above 0.10, was used to determine the severity of brain injury. After simulations, using the mass-based or the equal stress/velocity-based laws the CSDM10 in the human brain FE model was found to be 0.740, while the CSDM10 in the mouse brain FE model and human-material mouse brain model of 0.954 and 0.947 respectively. Accordingly, mouse brain showed much larger high strain areas and model materials did not affect the observation that applying traditional scaling laws to develop mouse head impacts would have significantly increased injury severity (Figure 3-2).

Human brain strain

Brain mass-based scaling law & Equal stress/velocity scaling law

Original mouse brain model

Human-material mouse brain model

CSDM10=0.740   CSDM10=0.954   CSDM10=0.947

Strain scale   0 ⌷⌷⌷⌷⌷⌷⌷⌷ 0.3
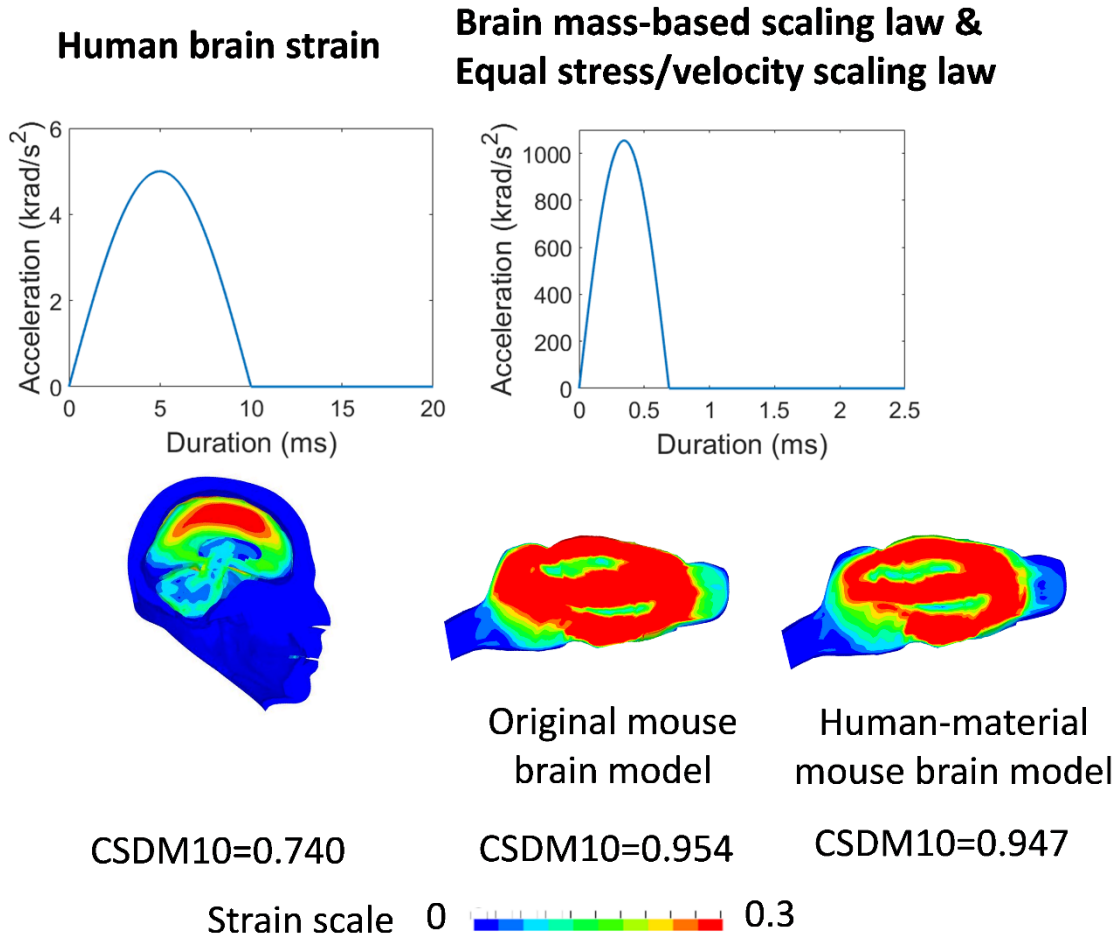
Figure 3-2 Evaluation of current scaling law. Applying traditional scaling induced larger strains in the mouse brain.

3.4.2   Scaled Mouse Brain Strain Data

Simulations were made of 78 mouse head rotations which were then used to calculate the relations between peak rotational acceleration and duration that defined rotational acceleration curves applied to drive FE brain models, peak rotational velocity was calculated by integrating rotational acceleration over time, and mouse brain strain. First, our simulations demonstrated that the CSDM10-based brain injury severity had a strong positive correlation with peak rotational velocity (R-squared = 1, Figure 3-3a). Constrained to the same-rotational-velocity data group, the CSDM10 value has a negative correlation with impact duration (R-squared = 1, Figure 3-3c) while the peak velocity

remained the same. Both rules indicated that longer durations and smaller peak rotational accelerations induced less damage. The same trends were also found in a modified mouse model with human brain material properties [47] (R-squared = 0.99 and 1 respectively, Figure 3-3a & c).

Peak rotational velocity VS. Brain strain responses

Duration VS. Brain strain responses
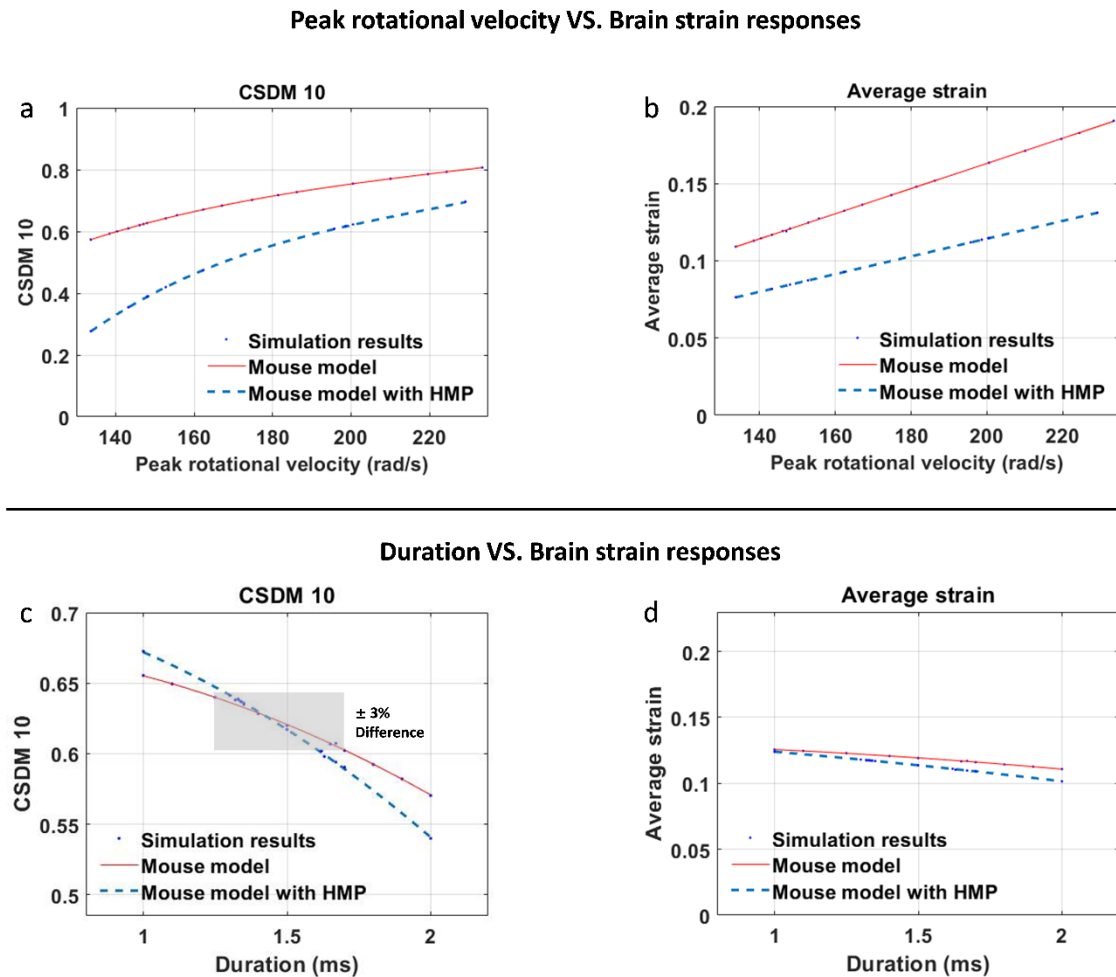
Figure 3-3 Relations between CSDM10, velocity and loading duration. The strain contour diagrams in the middle come from mouse model simulation results. (a) & (b) Model predicted CSDM10 and average strain increases with peak rotational velocity when the duration is set to be constant as 1.5 ms in both the mouse model and the modified mouse model. (c) & (d) Model predicted CSDM10 and average strain slightly decreases with the peak rotational velocity being set to be constant as 146 rad/s in the mouse model and 199 rad/s in the modified mouse model.

The scaling factor shows the ratio of peak velocity between loading conditions of mouse and human brain models. The scaling factors are different for different rotation directions as predicted. The largest scaling factor is 6.8 for axial rotation, followed by 5.8 for flexion and 4.6 for lateral bending (Table 4).

Table 4 Simulation results of mouse brain model and scaling factors between human and mouse.

	Mouse				Human	
Orientation	**Peak rot acceleration -duration[a]**	**Peak rot velocity[b]**	**CSDM10**	**Scaling factor (M/ H)** [c]	**Peak rot velocity[b]**	**CSDM10**
	173-1.65		0.72			
Flexion	193-1.5	184	0.74	5.8	31.8	0.74
	238-1.2		0.77			
	135-1.7		0.60			
Lateral bending	153-1.5	146	0.62	4.6	31.8	0.62
	184-1.25		0.64			
	180-1.87		0.77			
Axial rotation	225-1.5	215	0.80	6.8	31.8	0.80
	355-0.95		0.82			

Note. [a]The unit is $krad/s^2$ – ms; [b]The unit is rad/s; [c]M = Mouse (Peak rotational velocity), H = Human (Peak rotational velocity), Scaling factor is the ratio between mouse head peak rotational velocity and human head peak rotational velocity.

3.4.3   Effect of Mouse Brain Material

As for mouse brain FE model with human brain materials, the scaling factors become larger to 7.5, 6.3 and 7.1 for flexion, lateral bending, and axial rotation respectively (Table 5).

Table 5 Simulation results of human-material mouse brain model and scaling factors between human and mouse.

Orientation	Mouse				Human	
	Peak rot acceleration -duration[a]	Peak rot velocity[b]	CSDM10	Scaling factor (M/ H) [c]	Peak rot velocity[b]	CSDM10
Flexion	231-1.62		0.72			
	250-1.5	239	0.74	7.5	31.8	0.74
	274 -1.37		0.76			
Lateral bending	193-1.62		0.60			
	208-1.5	199	0.62	6.3	31.8	0.62
	233-1.34		0.64			
Axial rotation	189.5-1.86		0.77			
	235-1.5	224	0.80	7.1	31.8	0.80
	405-0.87		0.82			

Note. [a]The unit is krad/s^2 – ms; [b]The unit is rad/s; [c]M = Mouse (Peak rotational velocity), H = Human (Peak rotational velocity), Scaling factor is the ratio between mouse head peak rotational velocity and human head peak rotational velocity.

Meanwhile, the average strain showed a similar trend as CSDM did (R-squared > 0.99, Figure 3-3). The comparison of average strain results from human brain FE model, mouse brain FE model, and mouse brain FE model using human brain material materials are compared in Figure 3-4. In general, the differences were less than 10% during flexion and lateral bending modes.
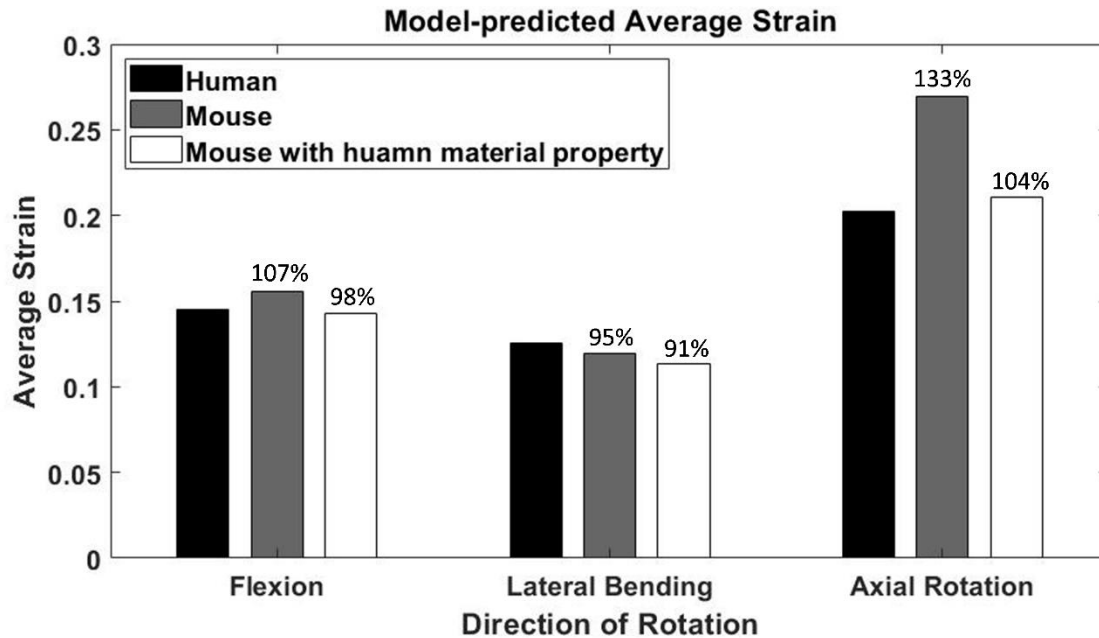
Figure 3-4 The comparison of predicted average strain between human, mouse and modified mouse models. The average strain around 0.15 indicates the injury severity is mild.

3.4.4 Strain Distribution Predicted by The Human Brain FE Model

In simulations for head impacts around the Y axis (causing flexion), the area that experienced MPS greater than 0.10 was the cortex with a maximum strain of 0.54. Additional scattered strains were also seen around the surface of the corpus callosum (0.23) and brainstem (0.31), with the cerebellum being less stretched (0.19) (Figure 3-5a and d). In simulations for lateral bending, the corpus callosum, thalamus, basal ganglia, cortex and cerebellum all experienced MPS larger than 0.1. The corpus callosum and cortex reached a maximum strain of 0.48 and 0.44 respectively (Figure 3-5b). Lastly, in simulations of injuries causing axial rotation, the most severe injury of all three cases, nearly all parts of the brain were affected. The cortex suffered the largest strain (0.74) at its surface. The corpus callosum had a strain of 0.37 and the hippocampus stood out in this loading condition with a strain of 0.46. The highest stretch always took place at the cortex except in lateral bending for which the corpus callosum experienced the highest strain (Figure 3-5c).

3.4.5 Strain Distribution Predicted by The Mouse Brain FE Model

Unlike the human brain FE model, MPS distributed in the mouse FE model showed a figure-eight pattern for simulations of injuries causing flexion (Figure 3-5a and d). The highest MPS (0.47) can be found in the cerebral cortex. The second highest strain was in the cerebellum (0.36). The brain stem, olfactory and pons experienced relatively small strains. In simulations of injuries causing lateral bending, the cortex had the highest strain of 0.38, while there were lower strains in the cerebellum (0.33) and thalamus (0.32) (Figure 3-5b). The worst damage among all mouse cases was predicted in simulations of injuries causing axial rotations, where the cortex and cerebellum had MPS of 0.8 and 0.75, respectively, but only a few portions of the thalamus and brain stem experiencing MPS over 0.10. Distributions of strain for simulations of injury were not significantly different between the mouse brain FE model and the mouse brain FE model using human brain material with the exception that strains were lower in injury simulations with axial rotation (Figure 3-5c).
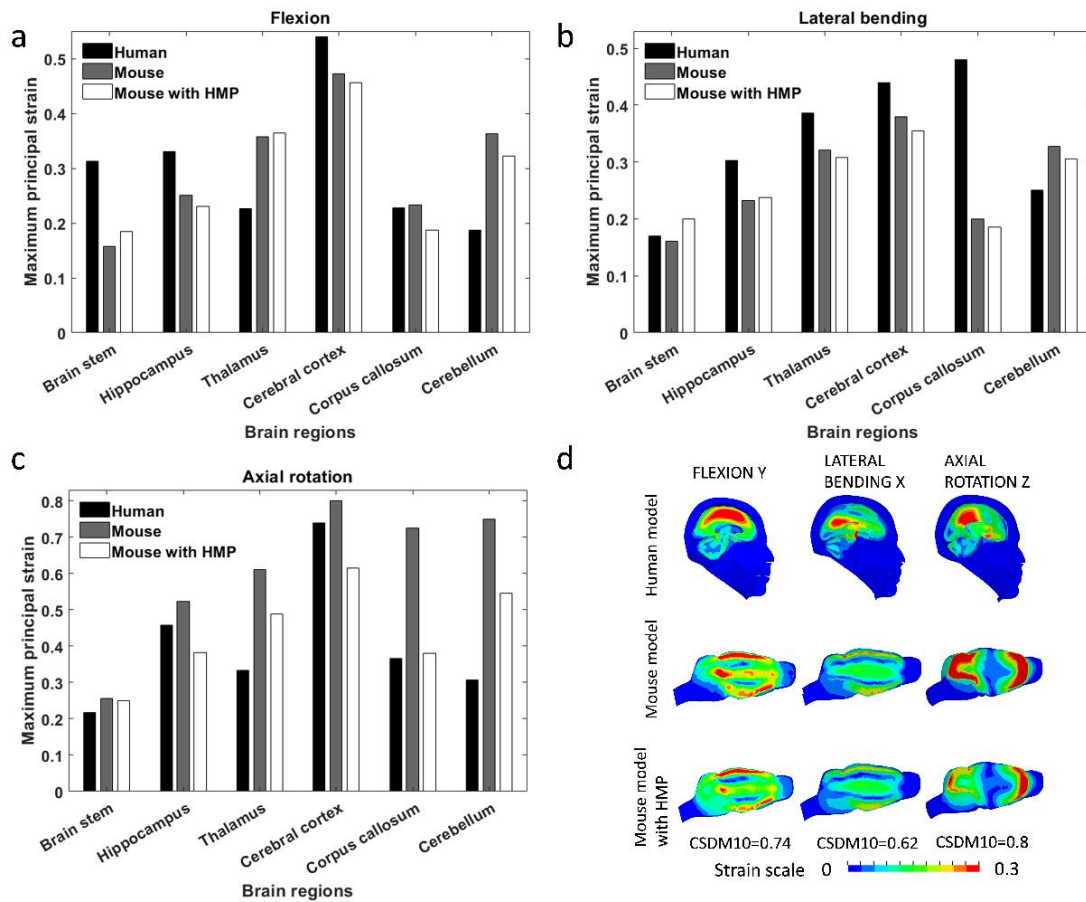
Figure 3-5 Predicted strain distribution. (a)(b)(c) Maximum principal strains for various brain regions in three rotational orientations including flexion, lateral bending, and axial rotation, respectively. (d) Predicted strain contour diagram of three models in three rotational orientations.

3.4.6   The Effect of Varying Durations

In reaching less than 3% difference of brain strain (CSDM10) between human and mouse brain, a duration of 1.37 to 1.62 ms was found for flexion loading, a duration of 1.34 to 1.62 ms was found for lateral bending, and a duration of 0.97 to 1.82 ms for axial rotation. With the same rotational velocity, the longer the duration, which corresponded to lesser peak acceleration, the smaller area in the brain would experience high-level strain (Figure 3-5c and d).

Results from simulations using flexion loading and durations of 0.75 ms, 1.5 ms, 3 ms, and 4.5 ms demonstrated a linear correlation between duration and scaling factors with a scope of 0.82 (R-squared = 0.99, Figure 3-6a). Under lateral bending, a similar linear relation was shown with a slope of 0.66 (R-squared = 0.99) while under axial rotation, scaling factors were similar for durations 1.5, 3.0 and 4.5 ms but smaller for a duration of 0.75 ms, forming a nonlinear relationship between duration and scaling factor. In general, larger scaling factors were calculated for loadings with a longer impact duration (Figure 3-6b).

a

The scaling factors for different durations

b
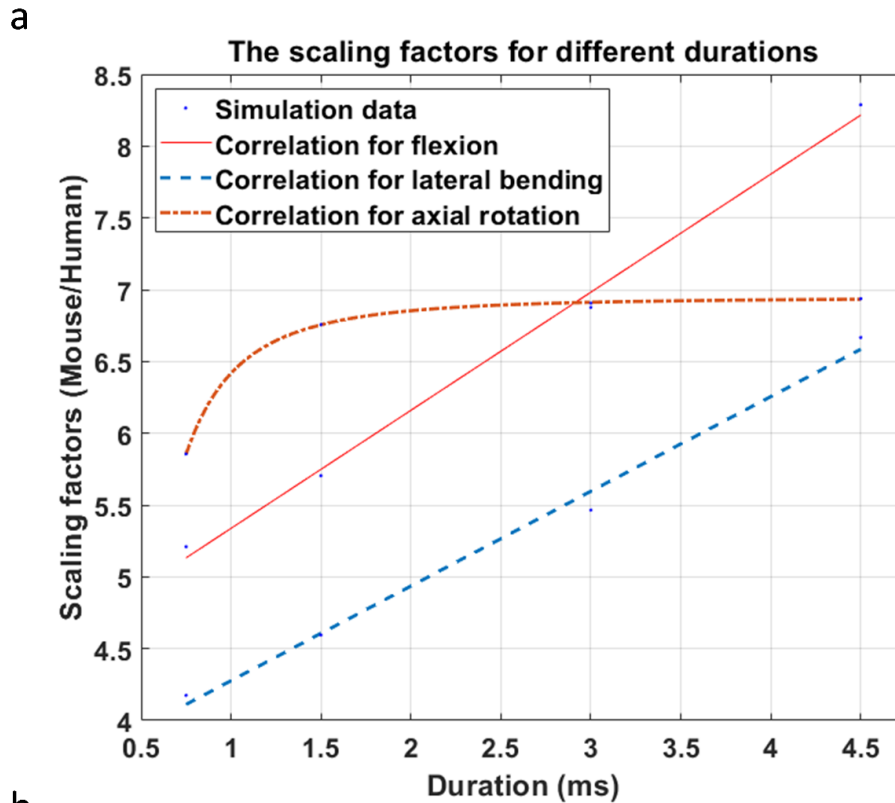
Duration (ms)		0.75	1.5	3	4.5
Scaling factor (M/H) [a]	F[b]	5.2	5.8	6.9	8.3
	L[c]	4.2	4.6	5.5	6.7
	A[d]	5.9	6.8	6.9	6.9

Note. [a]M = Mouse (Peak rotational velocity), H = Human (Peak rotational velocity);
[b]F = Flexion; [c]L = Lateral bending; [d]A = Axial rotation

Figure 3-6 The effect of duration during flexion loading. a) Scaling number increases linearly with duration. b) Summary of scaling factors for different durations.

3.5   Discussion

Mouse experiments are needed to study the pathophysiology of mTBI, but such studies are hampered by a lack of understanding of how laboratory impacts to the outside of the head translate into brain strain inside the head. This lack of understanding makes it

difficult to draw consistent correlations between laboratory mouse head impacts causing mTBI and the observed pathological and behavioral consequences from human head impacts. It also makes it difficult to evaluate the clinical relevance of the mouse mTBI models in use. Meanwhile, traditional scaling laws that did not take account of the shape differences between mouse and human brains were found invalid based on our data. To fill this gap, we simulated head impacts using human and mouse brain FE models to understand the internal brain strains, which are the direct cause of neuronal and functional damage and have been quantified in vitro [106, 107]. These analyses have led to 3 findings. First, we found that peak rotational velocity could serve as an efficient metric for scaling. Second, we developed direction-specific scaling laws, as the same rotational kinematics could result in various degrees of brain injury when applied to different rotational directions [108, 109]. Moreover, the geometry difference between human and mouse brain complicated the process of finding human-to-mouse scaling parameters. Our data supported measuring and scaling mouse head rotational velocities, which allow us to generate strain (CSDM10) in the mouse brain similar to that in the human brain with differences less than 3%. We calculated scaling factors 5.8 for scaling up human-head rotational velocities during flexion/extension loading, 4.6 for lateral bending, and 6.8 for axial rotation. Lastly, we investigated the applicable time duration range of developed laws and reported potential changes for shorter or longer mouse head impact durations. For example, the scaling factor changed from 5.8 for 1.5-ms impact to 8.3 for 4.5-ms impact. To the best of our knowledge, this study serves as a unique investigation correlating laboratory mouse brain strain to human brain strain, and provides a useful reference for mouse mTBI experiments.

We focused on simulating rotational kinematics of the closed-head impacts in this study, as our previous data supported that rotation was responsible for more than 95% of strains developed in the brain [91]. Doing so, we were able to capture the most important strain-related kinematics. In laboratory closed-head impact tests, no matter where the animal heads were hit, the induced linear and rotational kinematics were the culprits that induced brain responses and led to brain damage, especially for mild TBI impacts for which skull deformation is limited. Meanwhile, open-skull laboratory neurotrauma loadings such as CCI and FPI are still widely used, for which part of the skull was removed and mouse

cortical brain could experience strains up to 0.3 and higher in CCI [77] and around 0.10 in FPI [61]. The focus on rotational kinematics in this study was consistent with mouse models such as CHIMERA [31] and swine models, both focusing on inducing head rotations [110, 111]. Also, our scaling method was based on brain MPS and a limitation of this study needs to be acknowledged as the lack of investigation into damage related to the axon and vascular directions, which remain to be further investigated in the future.

Scaling studies have been conducted with the understanding of various degrees of brain injury [108, 109] and the acknowledgement of the geometry difference between human and animal brain. One example is to use natural frequency of the brain through a single-degree-of-freedom mechanical model [99]. One of the challenges is in such a method is to understand the frequency values which have diverse features [112]. On the other hand, the widely used mass-based scaling or same-stress-same-velocity approaches [42, 43] were found to generate different strains between the mouse and human brains, partially due to the huge geometrical differences between human and mouse brains, and hence found not fit for scaling mTBI mouse experiments. The brain strain or peak overpressure as a metric to evaluate the severity of blunt and blast-induced impact was used in the field [45, 83], as these brain internal responses directly cause injuries. In our work, the MPS-based CSDM was used to develop the unique mouse-to-human scaling laws.

The fixed impact duration of around 1.5 ms used in this study for Type 1 scaling has been used in models of rat TBI [97]. In addition, several rotational injury devices have been developed to induce mTBI in brain by exerting rotation [113-115]. In these studies, mouse post-injury behavior was examined through various methods such as elevated plus maze and rotarod performance tests. As various injury devices deliver different impact durations, we have expanded our scaling laws to accommodate both slightly changed durations (Type 2) and largely changed durations (Type 3). In all these Type 1, 2, and 3 scaling laws, the agreements between human and mouse brain strains were reached. Table 6 summarizes example cases of using the scaling laws developed in this study. For example, to induce mouse head impacts that mimics a 5 krad/s^2 & 10-ms flexion loading to the human head, various combinations of laboratory settings could be used such as 193 krad/s^2 & 1.5 ms, 347 krad/s^2 & 0.75 ms, 115 krad/s^2 & 3.0 ms, and 92 krad/s^2 & 4.5 ms.

Table 6 Example mouse head kinematics using calculated scaling factor.

Orientation	Human head Peak rot velocity[a]	Mouse head kinematics combinations Mouse head Peak rot acceleration – duration – peak rot velocity[b]			
		Duration (ms)			
		1-2	0.75	3.0	4.5
Flexion	31.8	173-1.65-184 193-1.5-184 238-1.2-184	347-0.75-166	115-3.0-220	92-4.5-264
Lateral bending	31.8	135-1.7-146 153-1.5-146 184-1.25-146	278-0.75-133	91-3-174	74-4.5-212
Axial rotation	31.8	180-1.87-215 225-1.5-215 355-0.95-215	390-0.75-186	115-3-220	77-4.5-221

Note. [a]The unit is rad/s – ms; [b]The unit is $krad/s^2$ – ms – rad/s.

3.6   Conclusion

To facilitate developing and understanding laboratory closed-head mouse mTBI experiments, which are designed to study human mTBI, we conducted a total of 201 simulations to investigate mouse and human brain strains during various impacts. Our data supported scaling human rotational velocity by 5.8, 4.6, and 6.8 under flexion/extension, lateral bending, and axial rotation, respectively, for mouse laboratory experiments. We also found that traditionally used mass-based or same-stress-same-velocity scaling laws did not apply to human-to-mouse brain injury scaling. Meanwhile, it should be noted that the application of the above scaling parameters best fit for mouse head impact durations of 1 to 2 ms, while with longer impact durations, larger scaling numbers are needed.

Chapter 4

4 Development of a Marmoset Brain Finite Element Model

4.1 Abstract

Laboratory animal traumatic brain injury (TBI) models are widely used to investigate the complex neuropathological effects after TBI. Among all animals, non-human primates (NHPs) share the majority of deoxyribonucleic acid (DNA) sequences and evolutionary traces as humans, with similar brain structures and injury pathologies between the both. In these NHPs, marmoset as the small type can undergo established transgenic/genome editing technologies, and hence can potentially serve as an effective animal model to study human TBI. To design a laboratory marmoset TBI model, a marmoset finite element (FE) brain model will be helpful. Hence, first, the marmoset brain and skull geometric data were obtained. Then, the feature-based multi-block approach was adopted to develop high-quality elements representing complex characteristics of the marmoset brain, including 21 brain anatomical regions such as the cortex, corpus callosum, cerebellum, brain stem thalamus, hypothalamus, pia, arachnoid, dura, cerebrospinal fluid (CSF) and three-layer skull. Lastly, rotational head motions along three anatomical axes were simulated to develop a new scaling law between marmoset and human TBI. Results demonstrated that applying scaling factors of 2.16, 2.04, and 1.98 to human head rotational velocities under flexion, lateral bending, and axial rotation, respectively, reproduced strain loading in the marmoset brain similar to that of the human brain under mild TBI-relevant impacts.

4.2 Introduction

Various laboratory animal traumatic brain injury (TBI) models have been developed and are being widely used. These animal TBI models include open-skull controlled cortical impact (CCI), open-skull fluid percussion injury (FPI), closed-head weight drop impact acceleration injury, and blast-induced brain injury. These animal models covered different brain injury mechanisms and mostly involved non-human mammals as the

subjects [53]. Among them, the most used are rodents including mice and rats, because of the advantages such as low cost and high reproducibility. Other larger animals such as swine and sheep have brains that are more comparable with the human brain in size, though the morphological and physiological heterogeneity and the high cost make large animals less popular for extensive studies of TBI [116].

Non-human primate (NHP) brains are more similar to human brains. The close biological kinship between NHP and human have already existed for 70 to 83 million years [117, 118]. The neural circuit and cognitive competence have changed during natural selection [119]. As a result, NHPs are considered an effective alternative in studying human brain pathology. Pioneering NHP TBI experiments have been conducted using rhesus monkeys [120], squirrel monkeys [121] and olive baboon [122], while marmoset TBI remains to be developed.

Marmoset, also referred to as Callithrix jacchus, belongs to one of the five new world (platyrrhine) primate families called Callitrichidae. There are more than 20 species, and most of them are small in size. Their body weight ranges from approximately 85 g (pygmy marmoset) to 860 g (Goeldi's marmoset). Also, the compact brain is suitable for the comprehensive analysis of neural circuits. Moreover, the frontal lobe of marmoset brain is more developed and more similar to that of human than other animals. In addition, marmoset has the characters of quick propagation with an average of 143 to 144 days [123], and a shorter lifetime than other large primate spices. Marmoset was chosen as the main focus of the brain/MINDS (Brain Mapping by Integrated Neurotechnologies for Disease Studies) national project in Japan. The goal of the brain/MINDS project was to develop a marmoset brain mapping for neuroscience study [29]. The MRI images of averaged marmoset brain template [27] provided a unique opportunity for finite element (FE) brain model development.

Brain strains, which are the direct cause of neuronal damage, could be studied for both animal and human TBI using finite element (FE) head models. Though physical models were used by researchers like Holbourn et al. [124], Margulies et al.[125], and Meaney et al. [126] to study brain responses, FE models, started from as early as the 1970's [127,

128], become a powerful and widely used tool. Since early 3-D, high-quality WSUBIM (WayneState University brain injury model) [129] and the KTH model [130], more human head models have been developed and even compared in a single study [131], in which 8 human FE brain models ([43, 47, 100, 132-136]) were used, including global human body model consortium (GHBMC) [47], imperial college model (IC) [132], kungliga tekniska högskolan (KTH) model [100], position and personalize advanced human body models for injury prediction (PIPER) model [133], simulated injury monitor (SIMon) model [43], total human model for safety (THUMS) model [134], university college dublin brain trauma model (UCDBTM) [135] and worcester head injury model (WHIM) [136].

Aside from human FE head models, animal FE head models have also been developed, though less in quantity compared to human FE models. Animal FE head models were developed for species used in laboratory, including rat [49], mouse [137], monkey [138], swine [139], and sheep [140]. For the NHP brain model, Tushar et al. recently developed a rhesus monkey head model, which simulates the brain cerebrum, cerebellum, stem, CSF, and skull [141]. The cerebrum structure was divided into white and grey matters. The main anatomy such as the corpus callosum, thalamus, and surface cortex was distinguished. Jacobo et al. developed a macaque head and neck FE model to study concussion criteria [45]. The same model was modified to a baboon model using a morphing technique. So far, a marmoset FE head model has yet to be reported.

This study aimed to develop a detailed and high-quality marmoset brain model, consistent with existing high-quality human and animal head models. The developed marmoset brain model was then combined with the previous human brain model to develop brain-strain-based scaling laws to help future marmoset TBI experiments. We hypothesized that the scaling factors between marmoset and human brain injury along all three rotational axes (coronal, lateral bending, and sagittal plane) could be similar due to close brain shapes between marmoset and human brains.

4.3   Methods

4.3.1   FE Marmoset Brain Model Development

4.3.1.1   Mesh Development

The marmoset brain geometry was developed based on magnetic resonance imaging (MRI) data in the RIKEN BSI research database [142], which represents the population-averaged standard template of the common marmoset brain. Main brain structures include white matter components, gray matter components, CSF, and the skull (Figure 4-1a and 1b). The 3D-Slicer [143] was used to convert MRI images to geometry model (Figure 4-1c). The feature-based multi-block approach [86] in ANSYS ICEM CFD (ANSYS, Canonsburg, Pennsylvania, U.S.) was used to create blocks (Figure 4-1d). This blocking technique avoided large angular distortions that usually happened at elements near curved brain surfaces or junctions. Another advantage of this block method is that the whole geometry was divided into relatively small blocks, fitting to the complex brain surfaces without compromising mesh quality. Besides, the mesh density can be controlled in each block, which means that the blocks are ready for flexible mesh size adjustment. After the block system was set up, high-quality hexahedral meshes were generated (Figure 4-1e). Then, the generated hexahedral mesh file was exported to HyperMesh (Altair Engineering, Troy, Michigan, United States) for adding skull, CSF, and meninge elements (Figure 4-1f). The mass of the FE brain model was checked to be consistent with literature data which was 8.15 grams [144]. The brain FE model is 31.8 mm in length and 24.2 mm in width, which is based on images. The pia, arachnoid, and dura membranes were modeled as shell elements, and CSF layers were modeled as the solid element which was offset from the pia shell layer. The thickness of the CSF layer was based on MRI images in the RIKEN BSI research database [142] with an average thickness of 0.33 mm. The skull thickness was also derived from images (Courtesy of Dr. Stefan Everling 's group) with an average thickness of 0.7 mm. The skull model has three layers. Finally, the FE brain model was undergoing rotational loading exercises to check its stability (Figure 4-1g) and analyze its strain predictions to check that there were no artificial strain predictions (Figure 4-1h). The final marmoset head model is composed of 21 parts including the cortex, corpus callosum, cerebellum, brain stem thalamus,

hypothalamus, pia, arachnoid, dura, CSF and three-layer skull. The dimension and location of brain functional regions were referenced to atlases developed by Liu et al. [145] and Senoo et al. [146].
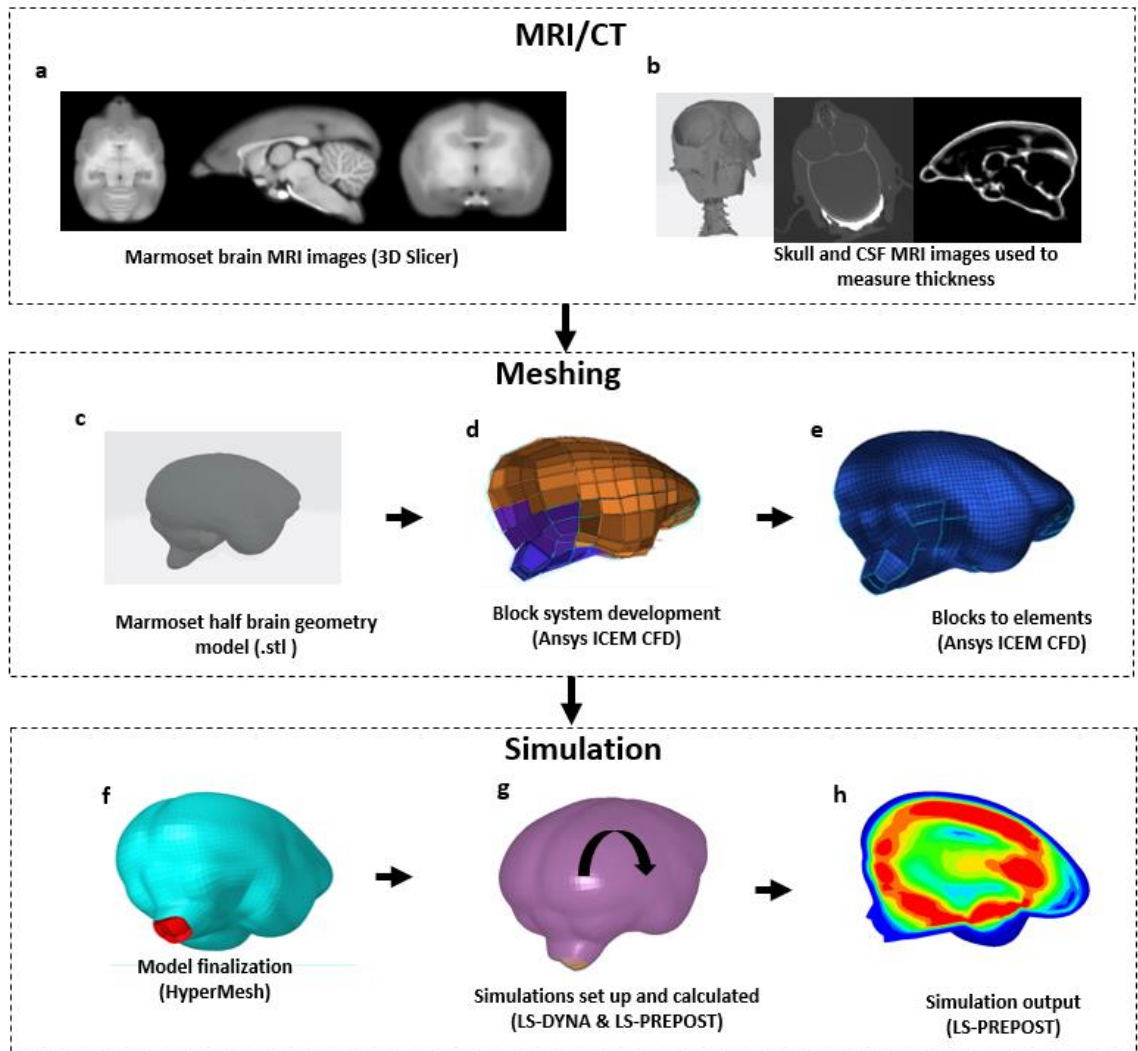
Figure 4-1 The flow diagram of the development of marmoset brain FE model.

4.3.1.2   Material property

Human and non-human primates share similar anatomical, cellular and genetic features, central nervous system tissues in human can be seen as a highly similar substitute for non-human primate brain tissue. With the lack of study related to marmoset brain tissue material testing, the material properties of brain tissue were referenced to the GHBMC

50th percentile male head model [47]. The densities of the brain, membrane, and skull bone were also referred to that in human. The total mass of the marmoset head model is 11.84 g, with 8.15 g for the brain model, 2.83 g for the skull model, 0.69 g for CSF, 0.17 g for the membranes. The brain model weight is consistent with literature about average male marmoset brain weight [147], for which a total of 82 male marmosets were measured immediately after euthanasia.

4.3.1.3   Mesh quality check

The mesh quality was assessed through several metrics. The first metric is Jacobian ratio, which monitors the distortion on element shape in comparison with an ideal shape element. For hexahedral element, the ideal shape is a cube, while for quadrilateral element, the ideal shape is a square. The ideal element will have a Jacobian ratio of 1, and worse quality will drop the number. The second metric is warpage, which checks how much a quadrilateral shell element or element faces in hexahedral element deviates from being planar, and worse quality will increase the number. In addition, the aspect ratio is the measure of an element's deviation from having all sides of equal length, a high aspect ratio can be found in slender elements. And the skew angle checks the angle between the normals of opposite edges, higher skew angle means worse mesh quality.

In total, 136,096 elements including 117,176 hexahedral and 18,920 quadrilateral shell were developed with high quality. For 3D hexahedral elements, all Jacobian values are above 0.56. The minimum element length is 0.040802 mm. 4% of elements have warpage of over 10 (maximum warpage is 41.4). All elements have an aspect ratio below 11.16. Two percent (2%) of elements have a minimum angle of less than 45 deg (minimum interior angle is 26.2 deg). 2% of elements have a maximum angle above 135 deg (maximum interior angle is 154.1 deg). 4% of elements have a skew angle above 40 deg (maximum skew angle is 62.0 deg).

For 2D quadrilateral elements, 0.3% of elements have a Jacobian less than 0.85 (minimum Jacobian is 0.77). 0.8% of elements have an edge length less than 0.2 mm (minimum length is 0.122260mm). 5% of elements have warpage over 10 (maximum warpage is 41.4). 4% of elements show an aspect ratio above 2 (maximum aspect ratio is

3.7). 1% of elements have a minimum angle less than 55 deg (minimum angle is 42.7 deg). 3% of elements have a maximum angle above 120 deg (maximum angle is 136.5 deg). 1% of elements have a skew angle above 35 deg (maximum skew angle is 45.6 deg).

4.3.1.4   Rotational head motion simulation

The rotational loading was applied to the center of gravity of the head model using *BOUNDARY_PERSCRIBED_MOTION_SET keyword using LS-PrePost. The rotational acceleration kinematics was simplified and described as a half-sine curve [91]. The standard loading duration is set as 10 ms. For all simulations, brain strains and cumulative strain damage measure (CSDM) with a cut-off threshold of 0.10 strain were analyzed. The marmoset head rotation simulations were then compared to human head rotational simulations to develop scaling laws using the previously established approach.

4.4   Results

A detailed marmoset FE brain model was developed. Using the developed model, a total of 39 simulations were computed. 15 for identifying the effect of small changes in injury duration, and 24 for evaluating the effect of large changes in injury duration. In addition, 3 typical human mTBI-relevant head impact simulations were conducted. A typical human head injury simulation took 2 CPUs approximately 8 hours to complete, while a marmoset brain model injury simulation took 2 CPUs approximately 3 hours to complete.

4.4.1   Strain-Based Scaling

The scaling factors of head peak rotational velocity for flexion, lateral bending, and axial rotation were found to be similar, which were 2.16, 2.04, and 1.98 respectively (Table 7). This is consistent with our previous assumption.

Table 7 Simulation results of mouse brain model and scaling factors between human and marmoset.

	Marmoset				Human	
Orientation	Peak rot acceleration -duration[a]	Peak rot velocity[b]	CSDM10	Scaling factor (M/ H) [c]	Peak rot velocity[b]	CSDM10
Flexion	31-3.5		0.72			

	36-3	184	0.74	2.16	31.8	0.74
	40-2.7		0.76			
Lateral bending	30-3.4		0.60			
	34-3	146	0.62	2.04	31.8	0.62
	36.5-2.8		0.64			
Axial rotation	25-4		0.77			
	33-3	215	0.80	1.98	31.8	0.80
	49.5-2		0.82			

Note. [a]The unit is krad/s^2 – ms; [b]The unit is rad/s; [c]M = Marmoset (Peak rotational velocity), H = Human (Peak rotational velocity), Scaling factor is the ratio between marmoset head peak rotational velocity and human head peak rotational velocity.

The average maximum principal strains (MPSs) from human head, marmoset brain, and mouse brain FE models are compared (Figure 4-2). The general pattern was that the average strains of the elements in the marmoset model were lower than the human and mouse model. The average strains for the mouse model were extremely direction-sensitive, which were higher during flexion and axial rotation and lower in lateral bending. The similar shape and corresponding rotational inertia between human and marmoset brains made the trends the same for all three directions between the marmoset and human brain. The differences were less than 10% during flexion and lateral bending. Overall, the average strain around 0.15 indicated the injury severity is mild.
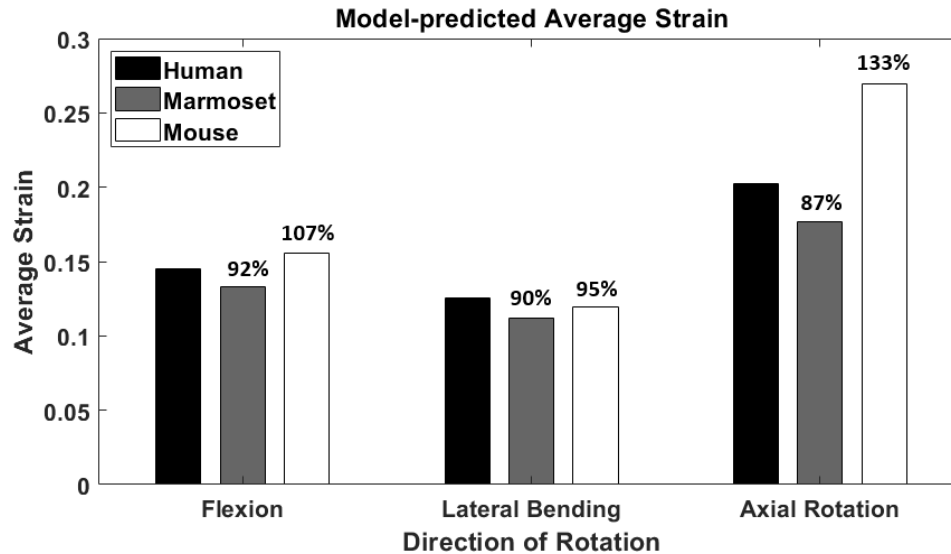
Figure 4-2 The comparison of predicted average strain between human, marmoset and mouse brain models. The percentage numbers located above the bar indicate the ratio when being compared to human cases.

4.4.2   Strain Distribution in Marmoset Brain

The predicted MPS in marmoset anatomical parts is generally lower (Figure 4-3). During flexion, the highest MPS (0.34) was found in the brainstem area, while there were lower strains in the cerebellum (0.31) and cortex (0.30). In lateral bending, the highest strain was also found in the brainstem (0.28). The cerebellum and cortex both reached a maximum principal strain of 0.27. In axial rotation, the cortex experienced the highest strain of 0.35, the cerebellum had a strain of 0.31, while the brainstem, hippocampus,

thalamus, and corpus callosum experienced strains around 0.
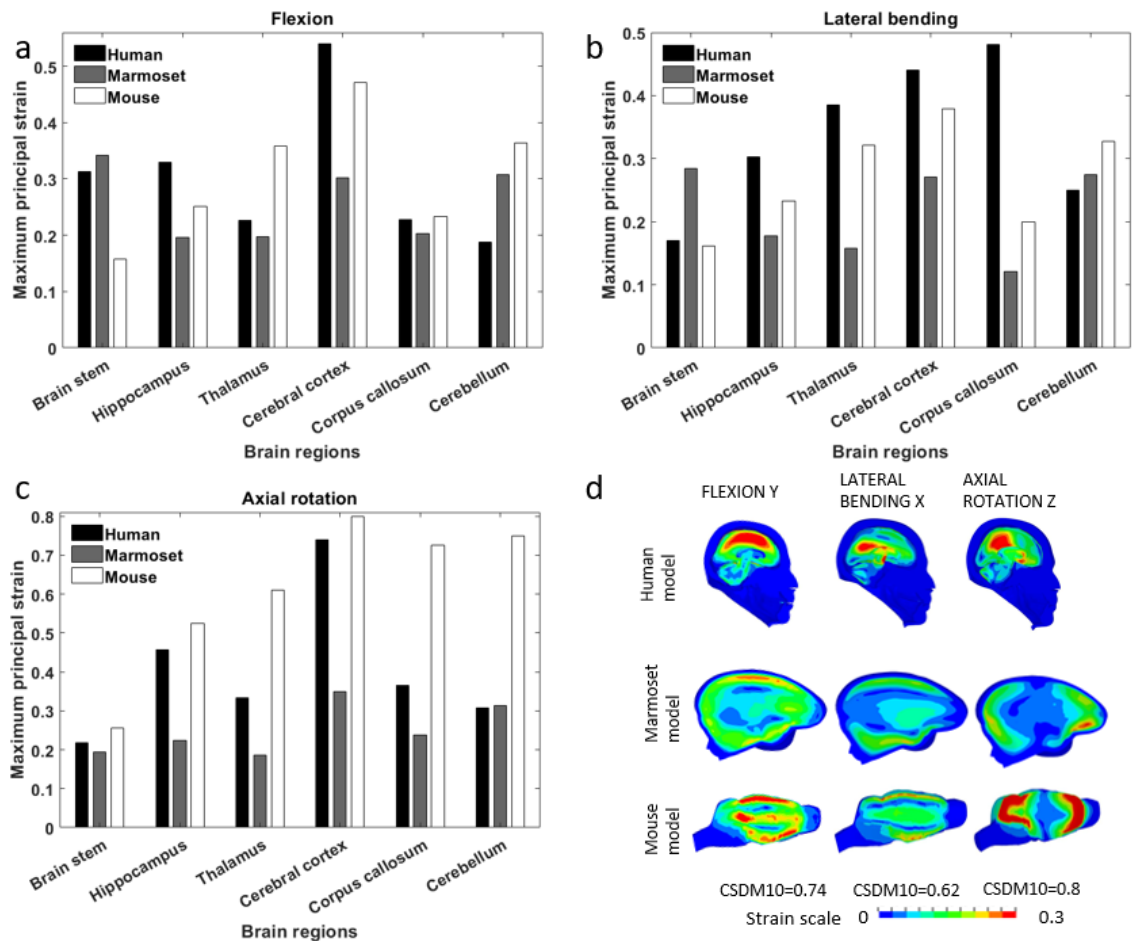
Figure 4-3 Predicted strain distribution. (a)(b)(c) Maximum principal strains for various brain regions in three rotational orientations including flexion, lateral bending, and axial rotation, respectively. (d) Predicted strain contour of three models in three rotational orientations.

4.5   Discussion

A unique marmoset FE brain model was developed using the multi-block approach to represent complex brain geometry with high-quality hexahedral elements. The marmoset FE model was then used to derive scaling factors for designing future marmoset TBI experiments. Our data suggested that marmoset could potentially be a valid TBI model when applying a scaling factor of around 2 to the collected human mTBI head rotational velocities. And these scaling factors are smaller than the numbers for the mouse which

are around 4 to 6, because the marmoset brain is around 20 times heavier in weight than the mouse brain. This is consistent with the report that the size of the brain has direct relations with injury tolerance [42, 148].

The predicted regional strains in marmoset and human brain models were not as close as we would expect. The potential explanation for this discrepancy is that, different from the human brain for which the cerebellum is relatively separated and confined, the marmoset cerebellum is closer to other brain regions. Hence, the human cerebellum experienced much less strains compared to other regions while the marmoset cerebellum experienced similar strains as the cortex.

There are several limitations of the current study. First, Human possess gyrencephalic brains featured with sulci and gyri on the brain surface, while this phenomenon is not significant in marmoset and rodent, as they belong to lissencephalic species and have a smooth cortex surface. Based on the literature, there exists a debate about whether the sulci and gyri protect the brain during impact or deteriorate the situation. One study compared the model without sulci and the model with sulci under the same rotational acceleration impulse, and showed that the presence of sulci reduced the average maximum principal strain by 12 percent [149]. Another research suggested that the presence of sulci and gyri would facilitate stress concentration and stress increase [150]. Nevertheless, both studies emphasized the role of sulci and gyri in influencing the severity of brain injury. Both marmoset brain model and the GHBM model were treated with smooth brain surfaces without gyri and sulci. Hence, the effect of gyri/sulci could not be investigated or compared.

Second, the falx cerebri and tentorium cerebelli structures could be developed in marmoset FE model (Figure 4-4). In the future improvement, scaling method or measurement is needed to get the accurate thickness and location of membranes for the model definition.
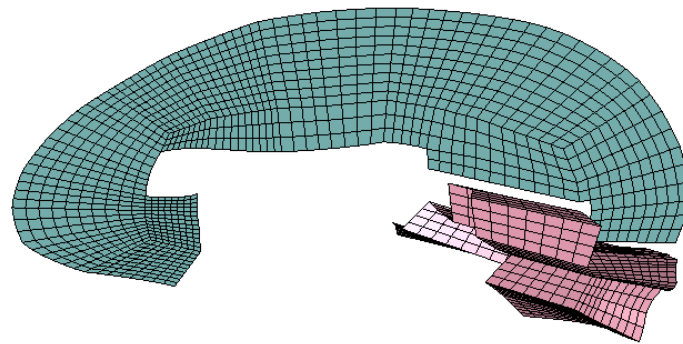
Figure 4-4 Mesh of falx and tentorium.

Third, there lacks experimental data, such as high-speed X-ray experiments [151-153] or brain surface deformation [154] to validate marmoset model predictions. Nevertheless, the high-quality hexahedral meshes were used together with established human brain material properties, which could help to predict reliable brain responses and establish meaningful scaling parameters.

4.6   Conclusions

A novel, 3D marmoset brain FE model was developed, representing 21 head anatomical components. The mesh quality of the model was ensured by adopting the feature-based multi-blocks technique to generate hexahedral meshes. 39 marmoset head rotations were simulated and used to develop the strain-based scaling law. Our calculations suggested that scaling the human peak rotational velocities with factors of 2.16, 2.04, and 1.98 for flexion, lateral bending, and axial rotation, respectively, would achieve identical brain strain response in marmoset and human brains. In the future, this marmoset brain FE model could serve as a tool for marmoset TBI experiment design and injury prediction

Chapter 5

5 Conclusion and Future Work

5.1 Summary

5.1.1 How Laboratory Animal TBI Models Mimic Real-World Human Brain Injury Scenarios

Traditional laboratory animal TBI models were developed without knowing brain strain responses, which are the direct causes of neuronal damage. Such limitation was addressed in this study. A novel GS method was developed to objectively quantify the focal-diffuse characteristics of brain injury, while traditionally whether a brain injury is categorized as diffuse or focal was done by subjective observation. We introduced two logics behind the GS method. First, the snake should always "eat" the element near it with the largest strain. Second, the snake could only go somewhere else after sweeping all elements at the focal injury spot. Doing so, we provided a novel and objective method to evaluate how diffuse a brain injury is. All of the animal and human TBI cases except for CCI showed some diffuse injury patterns. Concussion during football and whiplash during car accidents displayed a very similar diffuse pattern, which is because the rotational kinematics played a major role in these injuries.

In addition, the strain and strain rate were evaluated based on data extracted from six brain anatomical components. Our data indicate that human brain injury scenarios have somehow similar strain and strain rate levels, while, laboratory animal models showed much larger variances. This finding did not negate the contribution of traditional animal TBI models. Moreover, it is to emphasize the importance to be more human TBI relevant. Closed-head model such as CHIMERA was found to produce diffusion, strain, and strain rates most close to those experienced in human mTBI scenarios.

5.1.2 Brain-Strain-Based Scaling Law

Given the previous analysis, the brain-strain-based scaling law for closed-head mouse TBI model was investigated. The effectiveness of traditional scaling law described as

brain mass-based scaling and equal stress/velocity scaling was evaluated. To facilitate developing and understanding laboratory closed-head mouse mTBI experiments, which are designed to study human mTBI, we a total of 201 simulations were conducted to investigate mouse and human brain strains during various impacts. The CSDM 10 metric was used to evaluate brain injury severity. CSDM shows the volume proportion of elements that experienced MPS over the threshold and the number of it represents the overall brain damage. And the scaling factor was described as the ratio of rotational velocity, because it has the best correlation with brain strain metrics [91]. Our simulation data indicated that scaling human rotational velocity by 5.8, 4.6, and 6.8 under flexion/extension, lateral bending, and axial rotation for mouse TBI model respectively to reach comparable strain response. And we found that the CSDM10-based brain injury severity had a strong positive correlation with peak rotational velocity (Nonlinear R-squared = 1), and has a negative correlation with impact duration (Nonlinear R-squared = 1) while the peak velocity remained the same. But the MPS of various anatomical components is not similar, which may due to the different brain structures.

5.1.3   Development of Marmoset Brain FE Model

To make scaling law fit more species, a detailed marmoset brain FE model was developed. The FE model consists of 21 anatomical components, three meninges, CSF, and three-layer skull, the brain geometry and the thickness of CSF and skull were developed and set based on MRI images, and the layout of all brain functional parts referenced to the brain atlas [146]. In total, there are 117,176 hexahedral elements and 18,920 quadrilateral shell elements in this model, the mesh quality was checked as excellent, and the whole model weight was checked to be consistent with the data of real marmoset brain [147]. And the same method for developing brain-strain-based scaling law as used in chapter three was applied, and our data indicated that scaling human rotational velocity by 2.16, 2.04, and 1.98 under flexion/extension, lateral bending, and axial rotation for marmoset TBI model respectively. All scaling factors are around 2 without considerable difference, which due to the similar geometry between two species.

5.2   Limitation

The brain-strain-based scaling law used CSDM10 as the injury severity evaluator. The strain of 0.1 usually leads to very mild axonal damage, so our scaling law is developed to represent human mild TBI/ concussion rather than moderate to severe brain damage.

In addition, there lacked a direct validation study of the novel marmoset brain model. Nevertheless, the model was developed with great mesh quality and established human brain material property, which made the model fit for a marmoset-to-human scaling study.

5.3   Future work

5.3.1   Validation

Even though it is true that animal TBI models provide more opportunities to validate animal FE models than human, there still lacked marmoset TBI study data. And the material properties in marmoset brain model were referenced to GHBMC model settings. In the future, the correlation between mechanical input, model response, and experimental observation needs to be tested, to see how well marmoset brain FE model mimics real-world head impact biomechanics. As for now, the mesh was developed in good quality when compared with state-of-the-art finite element brain models. In addition, the similarity of brain tissue materials between human and non-human primates, and the MRI image-extracted geometry of marmoset brain FE model make element response reasonable and reliable.

In the future, clinical observations and corresponding kinematics of marmoset TBI experiments will be needed for validation through literature or cooperation between biological groups. And anatomical components division within the model has the potential to be more detailed and precise, which may improve the overall and local model responses because this will influence the proportion of gray matter to white matter.

5.3.2   Develop a scaling equation with moment of inertia

Current strain-based scaling law scaled rotational velocity, the scaling factors are direction and duration dependent, which limits the ease of application to some extent.

Since this thesis focused on rotational loadings, the moment of inertia could play a vital role to affect the brain tolerance to rotation. As shown in Table 8, the geometry disparity between three species is expressed by moment of inertia. Human and marmoset brains have more similar numbers in three directions, since they look more like a sphere shape in general, different from the mouse brain. Moue and marmoset brains have relatively lower numbers, so they required more energy to induce brain motions and then brain injuries. Putting moment of inertia into consideration is recommended.

Table 8 Brain FE model moment of inertia about center of gravity

Brain models	I_{xx}[a]	I_{yy}[b]	I_{zz}[c]
GHBMC	$2.0*10^{-3}$	$2.3*10^{-3}$	$2.5*10^{-3}$
Mouse	$4.2*10^{-9}$	$8.5*10^{-9}$	$9.7*10^{-9}$
Marmoset	$5.6*10^{-7}$	$4.1*10^{-7}$	$6.6*10^{-7}$

Note. X axis is along sagittal axis; Y axis is along frontal axis; Z axis is along longitudinal axis. [a,b,c]The unit is $kg*m^2$

5.3.3 Regional Response Comparison Between Marmoset, Mouse and Human

The regional strain values were compared in chapter three and four. The difference between three species was large. In the future, more brain injury metrics such as CSDM and average strain will be used to check injury severity in different anatomical parts.

5.3.4 Axon Fiber FE Model Integration

DAI is a frequent type of TBI, and the TBI symptoms getting worse when there are increasing amounts of damaged axons. As a result, the axonal strain becomes the most effective brain injury metric. Many studies integrate axon elements into the predefined animal or human brain FE model [155, 156], and the axonal strain will be effective to describe injury severity. So, in the future, human, mouse, and marmoset brain models with axon elements can be developed.

5.4 Novelty, Significance and Impact of Work

1. A novel, objective method to quantitatively evaluate the focal or diffuse properties of brain strain loading was developed. This method would overcome the limitations of the traditional method that uses subjective evaluation, and can provide a quantitative and

systematic comparison of various laboratory and real-world TBI cases to better understand TBI and better design laboratory animal TBI models.

2. Strain and strain rate responses between commonly used laboratory animal TBI model and real-world relevant human TBI cases were first systematically compared. The data demonstrated the limitations of traditional TBI models such as open-skull CCI in producing extremely high strain rates. Such knowledge would help better understand existing animal TBI models and promote future closed-head TBI experiments.

3. Brain-strain-based scaling relations among three species (human, mouse and marmoset) were developed. Traditional scaling law mainly took brain size and head kinematics into consideration [42, 43]. But with more brain injury mechanisms being revealed, it has been found that the axon strain directly affects symptoms and severity [157]. Our scaling law can make sure that brain tissues in all species experience a similar level of stretch which will lead to comparable clinical outcomes. And since the scaling law took the ratio of rotational velocity as scaling factor, we offered a guideline for researchers to design human TBI relevant animal experiments in lab.

4. This is the first study that developed a detailed and high-quality marmoset brain FE model. Such a model was used to derive scaling laws for marmoset TBI, which would contribute to future marmoset TBI lab tests.

References or Bibliography

[1]   M. C. Dewan *et al.*, "Estimating the global incidence of traumatic brain injury,"
        Journal of neurosurgery, vol. 130, no. 4, pp. 1-1097, 2018, doi:
        10.3171/2017.10.JNS17352.

[2]   A. B. Peterson, L. Xu, J. Daugherty, and M. J. Breiding, "Surveillance report of
        traumatic brain injury-related emergency department visits, hospitalizations, and
        deaths, United States, 2014," 2019.

[3]   "Report to Congress on mild traumatic brain injury in the United States; steps to
        prevent a serious public health problem," Report 2003.

[4]   K. Dams-O'Connor, L. E. Gibbons, J. D. Bowen, S. M. McCurry, E. B. Larson,
        and P. K. Crane, "Risk for late-life re-injury, dementia and death among
        individuals with traumatic brain injury: a population-based study," (in eng), *J
        Neurol Neurosurg Psychiatry,* vol. 84, no. 2, pp. 177-82, Feb 2013, doi:
        10.1136/jnnp-2012-303938.

[5]   L. Sakka, G. Coll, and J. Chazal, "Anatomy and physiology of cerebrospinal
        fluid," *European Annals of Otorhinolaryngology, Head and Neck Diseases,* vol.
        128, no. 6, pp. 309-316, 2011/12/01/ 2011, doi:
        https://doi.org/10.1016/j.anorl.2011.03.002.

[6]   S. S. Kenneth, *Anatomy & physiology: The unity of form and function*. McGraw-
        Hill, 2017.

[7]   H. Mao, "Chapter 12 - Modeling the Head for Impact Scenarios," in *Basic Finite
        Element Method as Applied to Injury Biomechanics*, K.-H. Yang Ed.: Academic
        Press, 2018, pp. 469-502.

[8]   A. A. Mercadante and P. Tadi, "Neuroanatomy, Gray Matter," in *StatPearls*.
        Treasure Island (FL): StatPearls Publishing

Copyright © 2021, StatPearls Publishing LLC., 2021.

[9]   K. H. Jawabri and S. Sharma, "Physiology, Cerebral Cortex Functions," in
        StatPearls. Treasure Island (FL): StatPearls Publishing

Copyright © 2021, StatPearls Publishing LLC., 2021.

[10]   S. Hofer and J. Frahm, "Topography of the human corpus callosum revisited—
        Comprehensive fiber tractography using diffusion tensor magnetic resonance
        imaging," *NeuroImage,* vol. 32, no. 3, pp. 989-994, 2006/09/01/ 2006, doi:
        https://doi.org/10.1016/j.neuroimage.2006.05.044.

[11] L.-L. Yang, Y.-N. Huang, and Z.-T. Cui, "Clinical features of acute corpus callosum infarction patients," (in eng), *International journal of clinical and experimental pathology,* vol. 7, no. 8, pp. 5160-5164, 2014.

[12] T. J. Torrico and S. Munakomi, "Neuroanatomy, Thalamus," in *StatPearls*. Treasure Island (FL): StatPearls Publishing

Copyright © 2021, StatPearls Publishing LLC., 2021.

[13] M. G. Pop, C. Crivii, and I. Opincariu, "Anatomy and function of the hypothalamus," *Hypothalamus in health and diseases,* 2018.

[14] E. Kandel, J. Schwartz, D. o. B. a. M. B. T. Jessell, S. Siegelbaum, and A. J. Hudspeth, *Principles of Neural Science, Fifth Edition*. Blacklick, UNITED STATES: McGraw-Hill Publishing, 2012.

[15] S. Mayor, "Mouse genome shows many disease genes shared with humans," (in eng), *BMJ : British Medical Journal,* vol. 325, no. 7376, pp. 1319-1319, 2002.

[16] H. Schröder, N. Moser, and S. Huggenberger, "The Mouse Thalamus," in *Neuroanatomy of the Mouse: An Introduction*, H. Schröder, N. Moser, and S. Huggenberger Eds. Cham: Springer International Publishing, 2020, pp. 171-203.

[17] H. Schröder, N. Moser, and S. Huggenberger, "The Mouse Cerebellum," in *Neuroanatomy of the Mouse: An Introduction*, H. Schröder, N. Moser, and S. Huggenberger Eds. Cham: Springer International Publishing, 2020, pp. 153-170.

[18] H. Schröder, N. Moser, and S. Huggenberger, "The Mouse Hippocampus," in *Neuroanatomy of the Mouse: An Introduction*, H. Schröder, N. Moser, and S. Huggenberger Eds. Cham: Springer International Publishing, 2020, pp. 267-288.

[19] J. P. McGann, "Poor human olfaction is a 19th-century myth," (in eng), *Science (New York, N.Y.),* vol. 356, no. 6338, p. eaam7263, 2017, doi: 10.1126/science.aam7263.

[20] S. Margulies and R. Hicks, "Combination Therapies for Traumatic Brain Injury: Prospective Considerations," (in English), *Journal of Neurotrauma,* vol. 26, no. 6, pp. 925-39, Jun 2009

2014-07-12 2009, doi: http://dx.doi.org/10.1089/neu.2008.0794.

[21] Y. P. Zhang, J. Cai, L. B. E. Shields, N. Liu, X.-M. Xu, and C. B. Shields, "Traumatic Brain Injury Using Mouse Models," *Translational Stroke Research,* vol. 5, no. 4, pp. 454-471, 2014/08/01 2014, doi: 10.1007/s12975-014-0327-0.

[22] S. R. Shultz *et al.*, "Clinical Relevance of Behavior Testing in Animal Models of Traumatic Brain Injury," *Journal of Neurotrauma,* vol. 37, no. 22, pp. 2381-2400, 2020/11/15 2019, doi: 10.1089/neu.2018.6149.

[23] N. Bye *et al.*, "Transient neuroprotection by minocycline following traumatic brain injury is associated with attenuated microglial activation but no changes in cell apoptosis or neutrophil infiltration," *Experimental Neurology,* vol. 204, no. 1, pp. 220-233, 2007/03/01/ 2007, doi: https://doi.org/10.1016/j.expneurol.2006.10.013.

[24] Y. Cao *et al.*, "Glutamate carboxypeptidase II gene knockout attenuates oxidative stress and cortical apoptosis after traumatic brain injury," *BMC Neuroscience,* vol. 17, no. 1, p. 15, 2016/04/18 2016, doi: 10.1186/s12868-016-0251-1.

[25] H. Shishido *et al.*, "Traumatic brain injury accelerates amyloid-β deposition and impairs spatial learning in the triple-transgenic mouse model of Alzheimer's disease," (in eng), *Neurosci Lett,* vol. 629, pp. 62-67, Aug 26 2016, doi: 10.1016/j.neulet.2016.06.066.

[26] N. Marklund, "Rodent Models of Traumatic Brain Injury: Methods and Challenges," in *Injury Models of the Central Nervous System: Methods and Protocols*, F. H. Kobeissy, C. E. Dixon, R. L. Hayes, and S. Mondello Eds. New York, NY: Springer New York, 2016, pp. 29-46.

[27] T. Hashikawa, R. Nakatomi, and A. Iriki, "Current models of the marmoset brain," *Neuroscience Research,* vol. 93, pp. 116-127, 2015/04/01/ 2015, doi: https://doi.org/10.1016/j.neures.2015.01.009.

[28] G. Paxinos, C. Watson, M. Petrides, M. Rosa, and H. Tokuno, *The marmoset brain in stereotaxic coordinates*. Elsevier Academic Press, 2012.

[29] H. Okano *et al.*, "Brain/MINDS: A Japanese National Brain Project for Marmoset Neuroscience," *Neuron,* vol. 92, no. 3, pp. 582-590, 2016/11/02/ 2016, doi: https://doi.org/10.1016/j.neuron.2016.10.018.

[30] J. W. Lighthall, "Controlled Cortical Impact: A New Experimental Brain Injury Model," *Journal of Neurotrauma,* vol. 5, no. 1, pp. 1-15, 1988/01/01 1988, doi: 10.1089/neu.1988.5.1.

[31] D. R. Namjoshi *et al.*, "Merging pathology with biomechanics using CHIMERA (Closed-Head Impact Model of Engineered Rotational Acceleration): a novel, surgery-free model of traumatic brain injury," *Molecular Neurodegeneration,* vol. 9, no. 1, 2014, doi: 10.1186/1750-1326-9-55.

[32] D. I. Graham, T. K. McIntosh, W. L. Maxwell, and J. A. R. Nicoll, "Recent Advances in Neurotrauma," *Journal of Neuropathology & Experimental Neurology,* vol. 59, no. 8, pp. 641-651, 2000, doi: 10.1093/jnen/59.8.641.

[33] S. V. Kabadi, G. D. Hilton, B. A. Stoica, D. N. Zapple, and A. I. Faden, "Fluid-percussion-induced traumatic brain injury model in rats," (in English), *Nature Protocols,* Report vol. 5, p. 1552+, 2010/09//

// 2010.

[34]   L. R. Gentry, J. C. Godersky, and B. Thompson, "MR imaging of head trauma: review of the distribution and radiopathologic features of traumatic lesions," *American Journal of Roentgenology,* vol. 150, no. 3, pp. 663-672, 1988.

[35]   C. A. Taylor, J. M. Bell, M. J. Breiding, and L. Xu, "Traumatic Brain Injury-Related Emergency Department Visits, Hospitalizations, and Deaths - United States, 2007 and 2013," (in eng), *Morbidity and mortality weekly report. Surveillance summaries (Washington, D.C. : 2002),* vol. 66, no. 9, pp. 1-16, 2017, doi: 10.15585/mmwr.ss6609a1.

[36]   A. C. Bain and D. F. Meaney, "Tissue-level thresholds for axonal damage in an experimental model of central nervous system white matter injury," (in eng), *J Biomech Eng,* vol. 122, no. 6, pp. 615-22, Dec 2000, doi: 10.1115/1.1324667.

[37]   L. F. Gabler, J. R. Crandall, and M. B. Panzer, "Development of a Metric for Predicting Brain Strain Responses Using Head Kinematics," *Annals of Biomedical Engineering,* vol. 46, no. 7, pp. 972-985, 2018/07/01 2018, doi: 10.1007/s10439-018-2015-9.

[38]   E. G. Takhounts, M. J. Craig, K. Moorhouse, J. McFadden, and V. Hasija, "Development of Brain Injury Criteria (BrIC)," *Stapp Car Crash Journal,* vol. 57, pp. 243-66, 2013.

[39]   A. Montanino and S. Kleiven, "Utilizing a Structural Mechanics Approach to Assess the Primary Effects of Injury Loads Onto the Axon and Its Components," *Frontiers in Neurology,* 10.3389/fneur.2018.00643 vol. 9, p. 643, 2018.

[40]   F. A. Bandak and R. H. Eppinger, "A Three-Dimensional Finite Element Analysis of the Human Brain Under Combined Rotational and Translational Accelerations," 1994. [Online]. Available: https://doi.org/10.4271/942215.

[41]   M. B. Panzer, G. W. Wood, and C. R. Bass, "Scaling in neurotrauma: How do we apply animal experiments to people?," vol. 261, no. Complete, pp. 120-126, 2014.

[42]   A. K. Ommaya, A. E. Hirsch, P. Yarnell, and E. H. Harris, "Scaling of experimental data on cerebral concussion in sub-human primates to concussion threshold for man," DAVID W TAYLOR NAVAL SHIP RESEARCH AND DEVELOPMENT CENTER BETHESDA MD …, 1967.

[43]   E. G. Takhounts, R. H. Eppinger, J. Q. Campbell, R. E. Tannous, E. D. Power, and L. S. Shook, "On the Development of the SIMon Finite Element Head Model," (in eng), *Stapp Car Crash J,* vol. 47, pp. 107-33, Oct 2003.

[44]   S. Lindstedt, "Body Size, Physiological Time, and Longevity of Homeothermic Animals," *Quarterly Review of Biology - QUART REV BIOL,* vol. 56, 03/01 1981, doi: 10.1086/412080.

[45]   T. Wu, J. Antona-Makoshi, A. Alshareef, J. S. Giudice, and M. B. Panzer, "Investigation of Cross-Species Scaling Methods for Traumatic Brain Injury Using Finite Element Analysis," *Journal of Neurotrauma,* 2019/10/03 2019.

[46]   K. H. Yang, H. Mao, C. Wagner, F. Zhu, C. C. Chou, and A. I. King, "Modeling of the Brain for Injury Prevention," ed. Berlin, Heidelberg: Springer Berlin Heidelberg, 2011, pp. 69-120.

[47]   H. Mao *et al.*, "Development of a finite element human head model partially validated with thirty five experimental cases," (in eng), *J Biomech Eng,* vol. 135, no. 11, p. 111002, Nov 2013, doi: 10.1115/1.4025101.

[48]   M. Iwamoto, Y. Nakahira, and H. Kimpara, "Development and validation of the total human model for safety (THUMS) toward further understanding of occupant injury mechanisms in precrash and during crash," *Traffic injury prevention,* vol. 16, no. sup1, pp. S36-S48, 2015.

[49]   H. Mao, L. Zhang, K. H. Yang, and A. I. King, "Application of a finite element model of the brain to study traumatic brain injury mechanisms in the rat," (in eng), *Stapp car crash journal,* vol. 50, pp. 583-600, Nov 2006, doi: 2006-22-0022 [pii].

[50]   S. Rowson *et al.*, "Rotational head kinematics in football impacts: an injury risk function for concussion," *Ann. Biomed. Eng.,* vol. 40, no. 1, pp. 1-13, Jan 2012, doi: 10.1007/s10439-011-0392-4.

[51]   F. Hernandez *et al.*, "Six Degree-of-Freedom Measurements of Human Mild Traumatic Brain Injury," *Annals of Biomedical Engineering,* vol. 43, no. 8, pp. 1918-1934, 2015/08/01 2015, doi: 10.1007/s10439-014-1212-4.

[52]   P. H. Chan *et al.*, "Transgenic Mice and Knockout Mutants in the Study of Oxidative Stress in Brain Injury," *Journal of Neurotrauma,* vol. 12, no. 5, pp. 815-824, 1995/10/01 1995, doi: 10.1089/neu.1995.12.815.

[53]   Y. Xiong, A. Mahmood, and M. Chopp, "Animal models of traumatic brain injury," (in eng), *Nat Rev Neurosci,* vol. 14, no. 2, pp. 128-42, Feb 2013, doi: 10.1038/nrn3407.

[54]   T. Skandsen, K. A. Kvistad, O. Solheim, I. H. Strand, M. Folvik, and A. Vik, "Prevalence and impact of diffuse axonal injury in patients with moderate and severe head injury: a cohort study of early magnetic resonance imaging findings and 1-year outcome," *Journal of neurosurgery,* vol. 113, no. 3, pp. 556-563, 2010, doi: 10.3171/2009.9.JNS09626.

[55]   T. M. J. C. Andriessen, B. Jacobs, and P. E. Vos, "Clinical characteristics and pathophysiological mechanisms of focal and diffuse traumatic brain injury," (in eng), *Journal of cellular and molecular medicine,* vol. 14, no. 10, pp. 2381-2392, 2010, doi: 10.1111/j.1582-4934.2010.01164.x.

[56]   A. Singh, Y. Lu, C. Chen, S. Kallakuri, and J. M. Cavanaugh, "A New Model of Traumatic Axonal Injury to Determine the Effects of Strain and Displacement Rates," (in English), *Stapp Car Crash Journal,* vol. 50, pp. 601-23, Nov 2006

2014-03-29 2006.

[57]   D. H. Smith, J. A. Wolf, T. A. Lusardi, V. M. Lee, and D. F. Meaney, "High tolerance and delayed elastic response of cultured axons to dynamic stretch injury," (in eng), *The Journal of neuroscience : the official journal of the Society for Neuroscience,* vol. 19, no. 11, pp. 4263-4269, 1999, doi: 10.1523/JNEUROSCI.19-11-04263.1999.

[58]   A. C. Bain, R. Raghupathi, and D. F. Meaney, "Dynamic Stretch Correlates to Both Morphological Abnormalities and Electrophysiological Impairment in a Model of Traumatic Axonal Injury," (in English), *Journal of Neurotrauma,* vol. 18, no. 5, pp. 499-511, May 2001

2014-07-12 2001, doi: http://dx.doi.org/10.1089/089771501300227305.

[59]   X. Ma, A. Aravind, B. J. Pfister, N. Chandra, and J. Haorah, "Animal Models of Traumatic Brain Injury and Assessment of Injury Severity," *Molecular Neurobiology,* vol. 56, no. 8, pp. 5332-5345, 2019/08/01 2019, doi: 10.1007/s12035-018-1454-5.

[60]   T. K. McIntosh *et al.*, "Traumatic brain injury in the rat: characterization of a lateral fluid-percussion model," (in eng), *Neuroscience,* vol. 28, no. 1, pp. 233-44, 1989.

[61]   H. Mao, L. Lu, K. Bian, F. Clausen, N. Colgan, and M. Gilchrist, "Biomechanical analysis of fluid percussion model of brain injury," vol. 77, 2018.

[62]   T. B. VanItallie, "Traumatic brain injury (TBI) in collision sports: Possible mechanisms of transformation into chronic traumatic encephalopathy (CTE)," (in eng), *Metabolism,* vol. 100s, p. 153943, Nov 2019, doi: 10.1016/j.metabol.2019.07.007.

[63]   G. Li, F. Wang, D. Otte, and C. Simms, "Characteristics of pedestrian head injuries observed from real world collision data," *Accident Analysis & Prevention,* vol. 129, pp. 362-366, 2019/08/01/ 2019, doi: https://doi.org/10.1016/j.aap.2019.05.007.

[64]   C. M. Marshall, H. Vernon, J. J. Leddy, and B. A. Baldwin, "The role of the cervical spine in post-concussion syndrome," *The Physician and Sportsmedicine,* vol. 43, no. 3, pp. 274-284, 2015/07/03 2015, doi: 10.1080/00913847.2015.1064301.

[65]   S. Rowson, G. Brolinson, M. Goforth, D. Dietter, and S. Duma, "Linear and angular head acceleration measurements in collegiate football," (in eng), *J Biomech Eng,* vol. 131, no. 6, p. 061016, Jun 2009, doi: 10.1115/1.3130454.

[66]   T. C. P. Sedan, "Tech Summary," 2016.

[67]   R. Watanabe, H. Miyazaki, Y. Kitagawa, and T. Yasuki, "Research of collision speed dependency of pedestrian head and chest injuries using human FE model (THUMS version 4)," in *22nd international technical conference on the enhanced safety of vehicles (ESV), WA*, 2011, pp. 11-0043.

[68]   G. P. Siegmund, B. E. Heinrichs, D. D. Chimich, and J. Lawrence, "Variability in Vehicle and Dummy Responses in Rear-End Collisions," *Traffic Injury Prevention,* vol. 6, no. 3, pp. 267-277, 2005/09/01 2005, doi: 10.1080/15389580590969427.

[69]   B. S. Elkin, J. M. Elliott, and G. P. Siegmund, "Whiplash Injury or Concussion? A Possible Biomechanical Explanation for Concussion Symptoms in Some Individuals Following a Rear-End Collision," (in eng), *J Orthop Sports Phys Ther,* vol. 46, no. 10, pp. 874-885, Oct 2016, doi: 10.2519/jospt.2016.7049.

[70]   U. S. D. o. T. F. A. Administration, "Task A14: UAS Ground Collision Severity Evaluation 2017-2019," 2019.

[71]   H. Mao *et al.*, "Development of a finite element human head model partially validated with thirty five experimental cases," *Journal of biomechanical engineering,* vol. 135, no. 11, pp. 111002-15, Nov 1 2013, doi: 10.1115/1.4025101.

[72]   J. M. Meythaler, J. D. Peduzzi, E. Eleftheriou, and T. A. Novack, "Current concepts: diffuse axonal injury-associated traumatic brain injury," (in eng), *Arch Phys Med Rehabil,* vol. 82, no. 10, pp. 1461-71, Oct 2001, doi: 10.1053/apmr.2001.25137.

[73]   Y. Chen, H. Mao, K. H. Yang, T. Abel, and D. F. Meaney, "A modified controlled cortical impact technique to model mild traumatic brain injury mechanics in mice," *Frontiers in neurology,* vol. 5, p. 100, 2014, doi: 10.3389/fneur.2014.00100.

[74]   Z. Y. Kerr, S. W. Marshall, H. P. Harding, Jr., and K. M. Guskiewicz, "Nine-year risk of depression diagnosis increases with increasing self-reported concussions in retired professional football players," (in eng), *Am J Sports Med,* vol. 40, no. 10, pp. 2206-12, Oct 2012, doi: 10.1177/0363546512456193.

[75]   P. McCrory *et al.*, "Consensus statement on concussion in sport: the 4th International Conference on Concussion in Sport held in Zurich, November 2012," *British Journal of Sports Medicine,* vol. 47, no. 5, p. 250, 2013.

[76] K. McInnes, C. L. Friesen, D. E. MacKenzie, D. A. Westwood, and S. G. Boe, "Mild Traumatic Brain Injury (mTBI) and chronic cognitive impairment: A scoping review.(Research Article)," *PLoS ONE,* vol. 12, no. 4, p. e0174847, 2017, doi: 10.1371/journal.pone.0174847.

[77] H. Mao, F. Guan, X. Han, and K. H. Yang, "Strain-based regional traumatic brain injury intensity in controlled cortical impact: a systematic numerical analysis," *Journal of Neurotrauma,* vol. 28, p. 2263+, 2020/4/17/ 2011.

[78] J. T. Cole *et al.*, "Craniotomy: True Sham for Traumatic Brain Injury, or a Sham of a Sham?," *Journal of Neurotrauma,* vol. 28, no. 3, pp. 359-369, 2020/08/04 2010.

[79] A. N. Bolton Hall, B. Joseph, J. M. Brelsfoard, and K. E. Saatman, "Repeated Closed Head Injury in Mice Results in Sustained Motor and Memory Deficits and Chronic Cellular Changes.(Report)," *PLoS ONE,* vol. 11, no. 7, 2016, doi: 10.1371/journal.pone.0159442.

[80] E. M. Fievisohn, V. S. S. S. Sajja, P. J. Vandevord, and W. N. Hardy, "Evaluation of Impact-Induced Traumatic Brain Injury in the Göttingen Minipig Using Two Input Modes," *Traffic Injury Prevention: Peer-Reviewed Journal for the 58th Annual Scientific Conference of the Association for the Advancement of Automotive Medicine (AAAM), October 2014,* vol. 15, no. S1, pp. S81-S87, 2014, doi: 10.1080/15389588.2014.929670.

[81] E. Armstrong, "A look at relative brain size in mammals," (in eng), *Neurosci Lett,* vol. 34, no. 2, pp. 101-4, Dec 30 1982, doi: 10.1016/0304-3940(82)90159-8.

[82] I. G. Bowen, E. R. Fletcher, D. R. Richmond, and A. Defense Atomic Support, *Estimate of man's tolerance to the direct effects of air blast*. Albuqueque, NM: Lovelace Foundation for Medical Education and Research (in English), 1968.

[83] G. Wood, M. Panzer, A. Yu, K. A. Rafaels, K. A. Matthews, and C. R. Bass, "Scaling in blast neurotrauma," *2013 IRCOBI Conference Proceedings - International Research Council on the Biomechanics of Injury,* pp. 549-558, 01/01 2013.

[84] A. Jean, M. K. Nyein, J. Q. Zheng, D. F. Moore, J. D. Joannopoulos, and R. Radovitzky, "An animal-to-human scaling law for blast-induced traumatic brain injury risk assessment," *Proceedings of the National Academy of Sciences,* vol. 111, no. 43, p. 15310, 2014, doi: 10.1073/pnas.1415743111.

[85] R. Saunders, X. G. Tan, and A. Bagchi, "On the Development of Interspecies Traumatic Brain Injury Correspondence Rules," *Military Medicine,* vol. 184, no. Supplement_1, pp. 181-194, 2019, doi: 10.1093/milmed/usy360.

[86] H. Mao, H. Gao, L. Cao, V. V. Genthikatti, and K. H. Yang, "Development of high-quality hexahedral human brain meshes using feature-based multi-block

approach," (in eng), *Comput Methods Biomech Biomed Engin,* vol. 16, no. 3, pp. 271-9, 2013, doi: 10.1080/10255842.2011.617005.

[87] J. M. Pleasant, S. W. Carlson, H. Mao, S. W. Scheff, K. H. Yang, and K. E. Saatman, "Rate of neurodegeneration in the mouse controlled cortical impact model is influenced by impactor tip shape: implications for mechanistic and therapeutic studies," (in eng), *J Neurotrauma,* vol. 28, no. 11, pp. 2245-62, Nov 2011, doi: 10.1089/neu.2010.1499.

[88] H. L. Cater, L. E. Sundstrom, and B. Morrison, "Temporal development of hippocampal cell death is dependent on tissue strain but not strain rate," *Journal of Biomechanics,* vol. 39, no. 15, pp. 2810-2818, 2006/01/01/ 2006, doi: https://doi.org/10.1016/j.jbiomech.2005.09.023.

[89] S. Rowson, J. G. Beckwith, J. J. Chu, and D. S. Leonard, "A six degree of freedom head acceleration measurement device for use in football," *Journal of applied biomechanics,* vol. 27, no. 1, pp. 8-14, 2011.

[90] S. M. Duma *et al.*, "Analysis of real-time head accelerations in collegiate football players," (in eng), *Clin J Sport Med,* vol. 15, no. 1, pp. 3-8, Jan 2005.

[91] K. Bian and H. Mao, "Mechanisms and variances of rotation-induced brain injury: a parametric investigation between head kinematics and brain strain," 2020.

[92] F. Bandak *et al.*, "Development of improved injury criteria for the assessment of advanced automotive restraint systems : II," (in English), Research Paper 1999.

[93] R. H. Eppinger, "Prediction of thoracic injury using measurable experimental parameters," in *Proc. 6th International Technical Conference on the Enhanced Safety of Vehicles*, 1976, vol. 6, pp. 770-779.

[94] S. M. Gentleman *et al.*, "Axonal injury: a universal consequence of fatal closed head injury?," (in eng), *Acta Neuropathol,* vol. 89, no. 6, pp. 537-43, 1995, doi: 10.1007/bf00571509.

[95] H. Mao, K. H. Yang, A. I. King, and K. Yang, "Computational neurotrauma--design, simulation, and analysis of controlled cortical impact model," (in eng), *Biomech Model Mechanobiol,* vol. 9, no. 6, pp. 763-72, Dec 2010, doi: 10.1007/s10237-010-0212-z.

[96] R. J. Fijalkowski, B. D. Stemper, F. A. Pintar, N. Yoganandan, M. J. Crowe, and T. A. Gennarelli, "New rat model for diffuse brain injury using coronal plane angular acceleration," (in eng), *J Neurotrauma,* vol. 24, no. 8, pp. 1387-98, Aug 2007, doi: 10.1089/neu.2007.0268.

[97] R. J. Fijalkowski, N. Yoganandan, J. Zhang, and F. A. Pintar, "A finite element model of region-specific response for mild diffuse brain injury," (in eng), *Stapp Car Crash J,* vol. 53, pp. 193-213, Nov 2009.

[98]   B. M. Knowles and C. R. Dennison, "Predicting Cumulative and Maximum Brain Strain Measures From HybridIII Head Kinematics: A Combined Laboratory Study and Post-Hoc Regression Analysis," vol. 45, no. 9, pp. 2146-2158, 2017.

[99]   L. F. Gabler, H. Joodaki, J. R. Crandall, and M. B. Panzer, "Development of a Single-Degree-of-Freedom Mechanical Model for Predicting Strain-Based Brain Injury Responses," *Journal of Biomechanical Engineering,* vol. 140, no. 3, 2018, doi: 10.1115/1.4038357.

[100]   S. Kleiven, "Predictors for Traumatic Brain Injuries Evaluated through Accident Reconstructions," *Stapp Car Crash Journal,* vol. 51, pp. 81-114, 2007.

[101]   D. B. MacManus, B. Pierrat, J. G. Murphy, and M. D. Gilchrist, "Region and species dependent mechanical properties of adolescent and young adult brain tissue," vol. 7, no. 1, p. 13729, 2017.

[102]   D. B. MacManus, B. Pierrat, J. G. Murphy, and M. D. Gilchrist, "Mechanical characterization of the P56 mouse brain under large-deformation dynamic indentation," vol. 6, no. 1, p. 21569, 2016.

[103]   A. Gefen, N. Gefen, Q. Zhu, R. Raghupathi, and S. S. Margulies, "Age-Dependent Changes in Material Properties of the Brain and Braincase of the Rat," *Journal of Neurotrauma,* vol. 20, no. 11, pp. 1163-1177, 2020/11/07 2003.

[104]   A. D. Sauerbeck *et al.*, "modCHIMERA: a novel murine closed-head model of moderate traumatic brain injury," vol. 8, no. 1, p. 7677, 2018.

[105]   K. Chen, H. Gu, L. Zhu, and D.-F. Feng, "A New Model of Repetitive Traumatic Brain Injury in Mice," (in English), *Frontiers in Neuroscience,* Original Research vol. 13, no. 1417, 2020-January-21 2020, doi: 10.3389/fnins.2019.01417.

[106]   B. Morrison, 3rd, B. S. Elkin, J. P. Dollé, and M. L. Yarmush, "In vitro models of traumatic brain injury," (in eng), *Annual Review of Biomedical Engineering,* Comparative Study vol. 13, pp. 91-126, Aug 15 2011, doi: 10.1146/annurev-bioeng-071910-124706.

[107]   E. W. Vogel, 3rd *et al.*, "Direct Observation of Low Strain, High Rate Deformation of Cultured Brain Tissue During Primary Blast," *Annals of biomedical engineering,* vol. 48, no. 4, pp. 1196-1206, Apr 2020, doi: 10.1007/s10439-019-02437-4.

[108]   L. S. Atlan, C. Smith, and S. S. Margulies, "Improved prediction of direction-dependent, acute axonal injury in piglets," (in eng), *Journal of neuroscience research,* vol. 96, no. 4, pp. 536-544, 2018, doi: 10.1002/jnr.24108.

[109]   S. Sullivan *et al.*, "Behavioral deficits and axonal injury persistence after rotational head injury are direction dependent," (in eng), *Journal of neurotrauma,* vol. 30, no. 7, pp. 538-545, 2013, doi: 10.1089/neu.2012.2594.

[110] K. D. Browne, X.-H. Chen, D. F. Meaney, and D. H. Smith, "Mild traumatic brain injury and diffuse axonal injury in swine," *Journal of Neurotrauma,* vol. 28, p. 1747+, 2021/2/13/ 2011.

[111] S. Sullivan *et al.*, "White matter tract-oriented deformation predicts traumatic axonal brain injury and reveals rotational direction-specific vulnerabilities," vol. 14, no. 4, pp. 877-896, 2015.

[112] K. Laksari, L. C. Wu, M. Kurt, C. Kuo, and D. C. Camarillo, "Resonance of human brain under head acceleration," *Journal of the Royal Society, Interface,* vol. 12, no. 108, pp. 20150331-20150331, 2015.

[113] B. D. Stemper *et al.*, "Behavioral Outcomes Differ between Rotational Acceleration and Blast Mechanisms of Mild Traumatic Brain Injury," (in English), *Frontiers in Neurology,* Original Research vol. 7, no. 31, 2016-March-14 2016, doi: 10.3389/fneur.2016.00031.

[114] A. A. Sabet, E. Christoforou, B. Zatlin, G. M. Genin, and P. V. Bayly, "Deformation of the human brain induced by mild angular head acceleration," *Journal of Biomechanics,* vol. 41, no. 2, pp. 307-315, 2008, doi: 10.1016/j.jbiomech.2007.09.016.

[115] D. K. Cullen *et al.*, "A Porcine Model of Traumatic Brain Injury via Head Rotational Acceleration," *Methods in molecular biology (Clifton, N.J.),* vol. 1462, pp. 289-324, 2016.

[116] R. Vink, "Large animal models of traumatic brain injury," *Journal of Neuroscience Research,* vol. 96, no. 4, pp. 527-535, 2021/04/05 2018.

[117] J. C. Izpisua Belmonte *et al.*, "Brains, genes, and primates," (in eng), *Neuron,* vol. 86, no. 3, pp. 617-631, 2015, doi: 10.1016/j.neuron.2015.03.021.

[118] D. Y. Anne, C. Matt, R. Maryellen, S. Kathleen, and V. Rytas, "Ancient Single Origin for Malagasy Primates," *Proceedings of the National Academy of Sciences - PNAS,* vol. 93, no. 10, pp. 5122-5126, 1996, doi: 10.1073/pnas.93.10.5122.

[119] J. H. Kaas, "The evolution of brains from early mammals to humans," *WIREs Cognitive Science,* https://doi.org/10.1002/wcs.1206 vol. 4, no. 1, pp. 33-45, 2013/01/01 2013, doi: https://doi.org/10.1002/wcs.1206.

[120] A. K. Ommaya, "Trauma to the nervous system," (in eng), *Ann R Coll Surg Engl,* vol. 39, no. 6, pp. 317-47, Dec 1966.

[121] A. K. Ommaya and A. E. Hirsch, "Tolerances for cerebral concussion from head impact and whiplash in primates," (in eng), *J Biomech,* vol. 4, no. 1, pp. 13-21, Jan 1971, doi: 10.1016/0021-9290(71)90011-x.

[122] T. A. Gennarelli, L. E. Thibault, J. H. Adams, D. I. Graham, C. J. Thompson, and R. P. Marcincin, "Diffuse axonal injury and traumatic coma in the primate," *Annals of Neurology,* vol. 12, no. 6, pp. 564-574, 1982, doi: 10.1002/ana.410120611.

[123] S. D. Tardif, D. A. Smucny, D. H. Abbott, K. Mansfield, N. Schultz-Darken, and M. E. Yamamoto, "Reproduction in captive common marmosets (Callithrix jacchus)," (in eng), *Comp Med,* vol. 53, no. 4, pp. 364-8, Aug 2003.

[124] A. Holbourn, "S.(1943). Mechanics of head injuries," *Lancet,* vol. 2, p. 438.

[125] S. S. Margulies, L. E. Thibault, and T. A. Gennarelli, "Physical model simulations of brain injury in the primate," *Journal of biomechanics,* vol. 23, no. 8, pp. 823-836, 1990.

[126] D. F. Meaney *et al.*, "Biomechanical analysis of experimental diffuse axonal injury," *Journal of neurotrauma,* vol. 12, no. 4, pp. 689-694, 1995.

[127] H. S. Chan, "Mathematical Model for Closed Head Impact," *SAE Transactions,* vol. 83, pp. 3814-3825, 1974.

[128] C. C. Ward and R. B. Thompson, "The Development of a Detailed Finite Element Brain Model," *SAE Transactions,* vol. 84, pp. 3238-3252, 1975.

[129] L. Zhang *et al.*, "Recent Advances in Brain Injury Research: A New Human Head Model Development and Validation," *Stapp car crash journal,* vol. 45, pp. 369-94, 12/01 2001.

[130] S. Kleiven and W. Hardy, "Correlation of an FE Model of the Human Head with Local Brain Motion--Consequences for Injury Prediction," *Stapp car crash journal,* vol. 46, pp. 123-44, 12/01 2002.

[131] M. Fahlstedt *et al.*, "Ranking and Rating Bicycle Helmet Safety Performance in Oblique Impacts Using Eight Different Brain Injury Models," *Annals of Biomedical Engineering,* vol. 49, no. 3, pp. 1097-1109, 2021/03/01 2021, doi: 10.1007/s10439-020-02703-w.

[132] M. Ghajari, P. J. Hellyer, and D. J. Sharp, "Computational modelling of traumatic brain injury predicts the location of chronic traumatic encephalopathy pathology," (in eng), *Brain,* vol. 140, no. 2, pp. 333-343, Feb 2017, doi: 10.1093/brain/aww317.

[133] X. Li and S. Kleiven, "Improved safety standards are needed to better protect younger children at playgrounds," (in eng), *Sci Rep,* vol. 8, no. 1, p. 15061, Oct 10 2018, doi: 10.1038/s41598-018-33393-z.

[134] N. Atsumi, Y. Nakahira, and M. Iwamoto, "Development and validation of a head/brain FE model and investigation of influential factor on the brain response

during head impact," *International journal of vehicle safety,* vol. 9, no. 1, pp. 1-23, 2016.

[135] A. Trotta, J. M. Clark, A. McGoldrick, M. D. Gilchrist, and A. N. Annaidh, "Biofidelic finite element modelling of brain trauma: Importance of the scalp in simulating head impact," *International Journal of Mechanical Sciences,* vol. 173, p. 105448, 2020.

[136] W. Zhao and S. Ji, "Displacement- and Strain-Based Discrimination of Head Injury Models across a Wide Range of Blunt Conditions," *Annals of Biomedical Engineering,* vol. 48, no. 6, pp. 1661-1677, 2020/06/01 2020, doi: 10.1007/s10439-020-02496-y.

[137] J. M. Pleasant, S. W. Carlson, H. Mao, S. Scheff, K. H. Yang, and K. E. Saatman, "Rate of Neurodegeneration in the Mouse Controlled Cortical Impact Model is Influenced by Impactor Tip Shape: Implications for Mechanistic and Therapeutic Studies," (in Eng), *Journal of neurotrauma,* vol. 28, pp. 2245-2262, Feb 22 2011, doi: 10.1089/neu.2010.1499.

[138] C. Ward, M. Chan, and A. Nahum, "Intracranial Pressure — A Brain Injury Criterion," *SAE Transactions,* vol. 89, pp. 3867-3880, 1980.

[139] Q. Zhu, M. Prange, and S. Margulies, "Predicting unconsciousness from a pediatric brain injury threshold," *Developmental neuroscience,* vol. 28, no. 4-5, pp. 388-395, 2006.

[140] R. W. G. Anderson, "A study on the biomechanics of axonal injury," 2000.

[141] T. Arora, L. Zhang, and P. Prasad, "Development of a subhuman primate brain finite element model to investigate brain injury thresholds induced by head rotation," SAE Technical Paper, 2020.

[142] A. Woodward *et al.*, "The Brain/MINDS 3D digital marmoset brain atlas," *Scientific Data,* vol. 5, no. 1, p. 180009, 2018/02/13 2018, doi: 10.1038/sdata.2018.9.

[143] A. Fedorov *et al.*, "3D Slicer as an image computing platform for the Quantitative Imaging Network," (in eng), *Magn Reson Imaging,* vol. 30, no. 9, pp. 1323-41, Nov 2012, doi: 10.1016/j.mri.2012.05.001.

[144] "Organ weight data in juvenile and adult marmosets (Callithrix jacchus)," *Laboratory Animals,* vol. 15, no. 4, pp. 385-388, 1981/10/01 1981, doi: 10.1258/002367781780952816.

[145] C. Liu *et al.*, "A resource for the detailed 3D mapping of white matter pathways in the marmoset brain," *Nature Neuroscience,* vol. 23, no. 2, pp. 271-280, 2020/02/01 2020, doi: 10.1038/s41593-019-0575-0.

[146]   A. Senoo, H. Tokuno, and C. Watson, "Mini-atlas of the marmoset brain," *Neuroscience Research,* vol. 93, pp. 128-135, 2015/04/01/ 2015, doi: https://doi.org/10.1016/j.neures.2014.12.014.

[147]   P. F. Wadsworth, D. A. Budgett, and M. L. Forster, "Organ weight data in juvenile and adult marmosets (Callithrix jacchus)," (in eng), *Lab Anim,* vol. 15, no. 4, pp. 385-8, Oct 1981, doi: 10.1258/002367781780952816.

[148]   "Animal models of traumatic brain injury: A review," *Australian veterinary journal.,* vol. 79, pp. 628-633, 2001.

[149]   "Can sulci protect the brain from traumatic injury?," *Journal of biomechanics.,* vol. 42, pp. 2074-2080, 2009.

[150]   "Biomechanics of traumatic brain injury: Influences of the morphologic heterogeneities of the cerebral cortex," *Annals of biomedical engineering.,* vol. 36, pp. 1203-1215, 2008.

[151]   W. N. Hardy, C. D. Foster, M. J. Mason, K. H. Yang, A. I. King, and S. Tashman, "Investigation of Head Injury Mechanisms Using Neutral Density Technology and High-Speed Biplanar X-ray," (in eng), *Stapp Car Crash J,* vol. 45, pp. 337-68, Nov 2001.

[152]   W. N. Hardy *et al.*, "A study of the response of the human cadaver head to impact," (in eng), *Stapp car crash journal,* vol. 51, pp. 17-80, 2007.

[153]   T. Whyte *et al.*, "Technique and preliminary findings for in vivo quantification of brain motion during injurious head impacts," *Journal of Biomechanics,* vol. 95, p. 109279, 2019/10/11/ 2019, doi: https://doi.org/10.1016/j.jbiomech.2019.07.023.

[154]   D. I. Shreiber *et al.*, "Experimental Investigation of Cerebral Contusion: Histopathological and Immunohistochemicc Evaluation of Dynamic Cortical Deformation," *Journal of Neuropathology & Experimental Neurology,* vol. 58, no. 2, pp. 153-164, 1999, doi: 10.1097/00005072-199902000-00005.

[155]   T. Wu, M. Hajiaghamemar, J. S. Giudice, A. Alshareef, S. S. Margulies, and M. B. Panzer, "Evaluation of Tissue-Level Brain Injury Metrics Using Species-Specific Simulations," *Journal of Neurotrauma,* 2021, doi: 10.1089/neu.2020.7445.

[156]   Y. Levy, "Computational Modeling of the Human Brain for mTBI Prediction and Diagnosis," 2020.

[157]   I. M. Medana and M. M. Esiri, "Axonal damage: a key predictor of outcome in human CNS diseases," *Brain,* vol. 126, no. 3, pp. 515-530, 2003, doi: 10.1093/brain/awg061.

.

Curriculum Vitae

Name: Xingyu Liu

Post-secondary Education and Degrees:

University of Jinan
Jinan, Shandong, China
2014-2018 B.Eng.

Western University
London, Ontario, Canada
2018-2019 M.Eng.

Western University
London, Ontario, Canada
2019-2021 M.E.Sc.

Related Work Experience

Teaching Assistant
Western University
2019-2021

Research Assistant
Western University
2019-2021

Publications:

1. Liu X et al., "Developing Brain-Strain-Based Scaling to Inform the Clinical Relevance of Mouse Models of Concussion Induced by Rotation," BMC Biomedical Engineering. (2021), (Under Reviewing)
2. Liu X. Developing Brain Strain-Based Scaling Law Between Mice and Human for Relating Real-World Concussive Impacts in Lab. BMES (2020), (Virtual poster)
3. Dickey GJ et al., "Identifying Vulnerable Impact Locations to Reduce the Occurrence of Deadly Commotio Cordis Events in Children's Baseball - A Computational Approach," Journal of Biomechanical Engineering. (2021)
4. Xu X. et al., "Repetitive mild traumatic brain injury in mice triggers a slowly developing cascade of long-term and persistent behavioral deficits and pathological changes," Acta Neuropathologica Communications. (2021)